Cell Reports

Article

Interplay between Liver X Receptor and Hypoxia Inducible Factor 1α Potentiates Interleukin-1β Production in Human Macrophages

Graphical Abstract

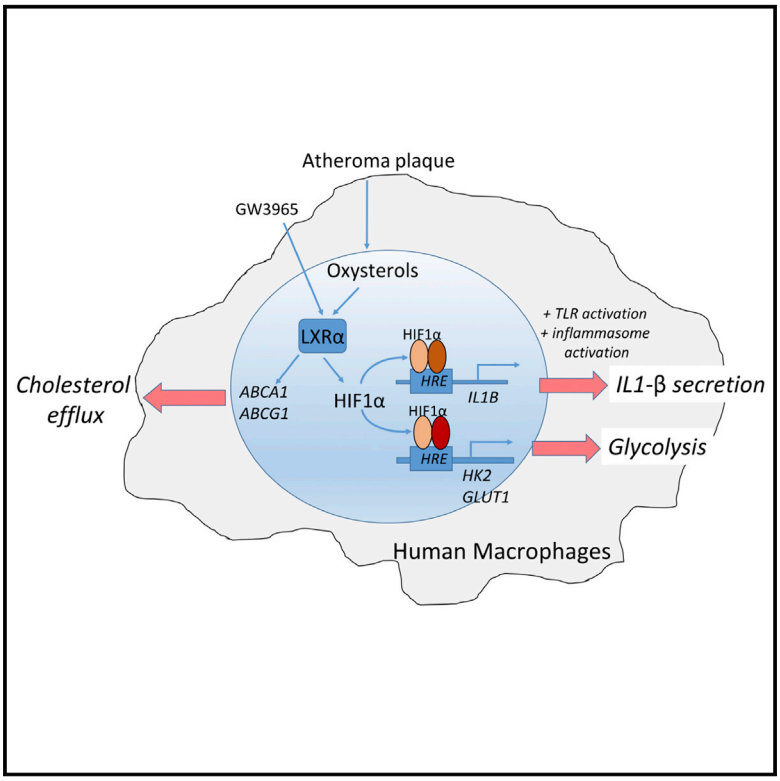

Highlights

- LXR agonists selectively increase *IL1B* mRNA levels in human macrophages *in vitro*
- The impact of LXR on IL-1β is dependent on HIF-1α
- LXR agonists activate other HIF-1α-dependent pathways, including glycolysis
- *IL1B* induction by atheroma plaque homogenates is blunted by LXR antagonists

Authors

Louise Ménégaut, Charles Thomas, Antoine Jalil, ..., Philippe Saas, Laurent Lagrost, David Masson

Correspondence

david.masson@chu-dijon.fr

In Brief

Ménégaut et al. show that liver X receptor (LXR) agonists selectively increase *IL1β* mRNA levels independently of TLR activation. This effect, restricted to human macrophages, is mediated by an activation of hypoxia inducible factor (HIF) 1α through LXR. Accordingly, LXR agonists also potentiate other HIF-1α-dependent pathways, such as glycolysis.

Ménégaut et al., 2020, Cell Reports *31*, 107665
May 19, 2020
https://doi.org/10.1016/j.celrep.2020.107665

CellPress

Cell Reports

CellPress
OPEN ACCESS

Article

Interplay between Liver X Receptor and Hypoxia Inducible Factor 1α Potentiates Interleukin-1β Production in Human Macrophages

Louise Ménégaut,[1,2,3,4] Charles Thomas,[1,2,3] Antoine Jalil,[1,2,3] Jean Baptiste Julla,[5] Charlène Magnani,[1,2,3] Adam Ceroi,[6,7] Louise Basmaciyan,[8,9] Adélie Dumont,[1,2,3] Wilfried Le Goff,[10] Mano Joseph Mathew,[5] Cédric Rébé,[1,2,3,11] Valentin Dérangère,[1,2,3,11] Aline Laubriet,[12] Valentin Crespy,[12] Jean-Paul Pais de Barros,[1,2,3,13] Eric Steinmetz,[12] Nicolas Venteclef,[5] Philippe Saas,[6,7] Laurent Lagrost,[1,2,3] and David Masson[1,2,3,4,14,*]

[1]Université Bourgogne Franche-Comté, LNC UMR1231, 21000 Dijon, France
[2]INSERM, LNC UMR1231, 21000 Dijon, France
[3]FCS Bourgogne-Franche Comté, LipSTIC LabEx, 21000 Dijon, France
[4]CHRU Dijon Bourgogne, Laboratory of Clinical Chemistry, 21000 Dijon, France
[5]Centre de Recherche des Cordeliers, INSERM, Université de Paris, IMMEDIAB Laboratory, 75006 Paris, France
[6]Université Bourgogne Franche-Comté, EFS Bourgogne Franche-Comté, INSERM, UMR1098, 25000 Besançon, France
[7]FCS Bourgogne-Franche Comté, LipSTIC LabEx, 25000 Besançon, France
[8]UMR A PAM, Équipe Vin, Aliment, Microbiologie, Stress, Université Bourgogne Franche-Comté, AgroSup Dijon, 21078 Dijon Cedex, France
[9]Parasitology-Mycology Department, University Hospital of Dijon, 21000 Dijon, France
[10]Sorbonne Université, Inserm, Institute of Cardiometabolism and Nutrition (ICAN), UMR_S1166, Hôpital de la Pitié, Paris 75013, France
[11]Centre Georges-François Leclerc, Cancer Biology Research Platform, 21000 Dijon, France
[12]CHRU Dijon Bourgogne, Department of Cardiovascular Surgery, 21000 Dijon, France
[13]Lipidomic Analytic Platform, UBFC, 21000 Dijon, France
[14]Lead Contact
*Correspondence: david.masson@chu-dijon.fr
https://doi.org/10.1016/j.celrep.2020.107665

SUMMARY

Low-grade inflammation is constitutive of atherosclerosis, and anti-inflammatory therapy inhibiting interleukin-1β (IL-1β) reduces the rate of cardiovascular events. While cholesterol accumulation in atheroma plaque and macrophages is a major driver of the inflammatory process, the role of the LXR cholesterol sensors remains to be clarified. Murine and human macrophages were treated with LXR agonists for 48 h before Toll-like receptor (TLR) stimulation. Unexpectedly, we observe that, among other cytokines, LXR agonists selectively increase *IL1B* mRNA levels independently of TLR activation. This effect, restricted to human macrophages, is mediated by activation of HIF-1α through LXR. Accordingly, LXR agonists also potentiate other HIF-1α-dependent pathways, such as glycolysis. Treatment of human macrophages with carotid plaque homogenates also leads to induction of *IL1B* in an LXR-dependent manner. Thus, our work discloses a mechanism by which cholesterol and oxysterols trigger inflammation in atherosclerosis. This suggests perspectives to target IL-1β production in atherosclerotic patients.

INTRODUCTION

Low-grade inflammation is constitutive of all stages of atherosclerosis. While cholesterol-lowering drugs such as statins and PCSK9 inhibitors reduce cardiovascular morbidity and mortality, strategies aimed at inhibiting inflammatory cytokines such as interleukin-1 beta (IL-1β) may provide additional benefits and open a new era in the field of cardiovascular disease (CVD) (Libby et al., 2009; Ridker et al., 2017). Although the origins of inflammation in atherosclerosis are multiple, cholesterol accumulation in atheroma plaque and macrophages appears to play a prominent role in the inflammatory process (Tall and Yvan-Charvet, 2015). For instance, cholesterol carriers such as oxidized low-density lipoproteins (oxLDLs) stimulate Toll-like receptor (TLR) signaling pathways, while cholesterol crystals activate the inflammasome and the subsequent release of IL-1β from macrophages (Stewart et al., 2010; Duewell et al., 2010). Liver X receptors (LXRs) represent an essential link between cholesterol accumulation and inflammatory response in macrophages (Joseph et al., 2003). These nuclear receptors are activated by cholesterol derivatives such as oxysterols and desmosterol, compounds that accumulate in cells after cholesterol loading (Spann et al., 2012; Wang and Tontonoz, 2018). In turn, LXRs activate genes that limit cholesterol accumulation by stimulating cholesterol efflux and inhibiting cholesterol uptake. Interestingly, LXRs also modulate the inflammatory response of macrophages by several distinct mechanisms. First, it was shown that LXRs suppress the expression of NF-κB- and AP-1-responsive genes by a trans-repression mechanism common to other nuclear receptors such as PPARs and involving ligand-dependent SUMOylation (Venteclef et al., 2010; Ghisletti

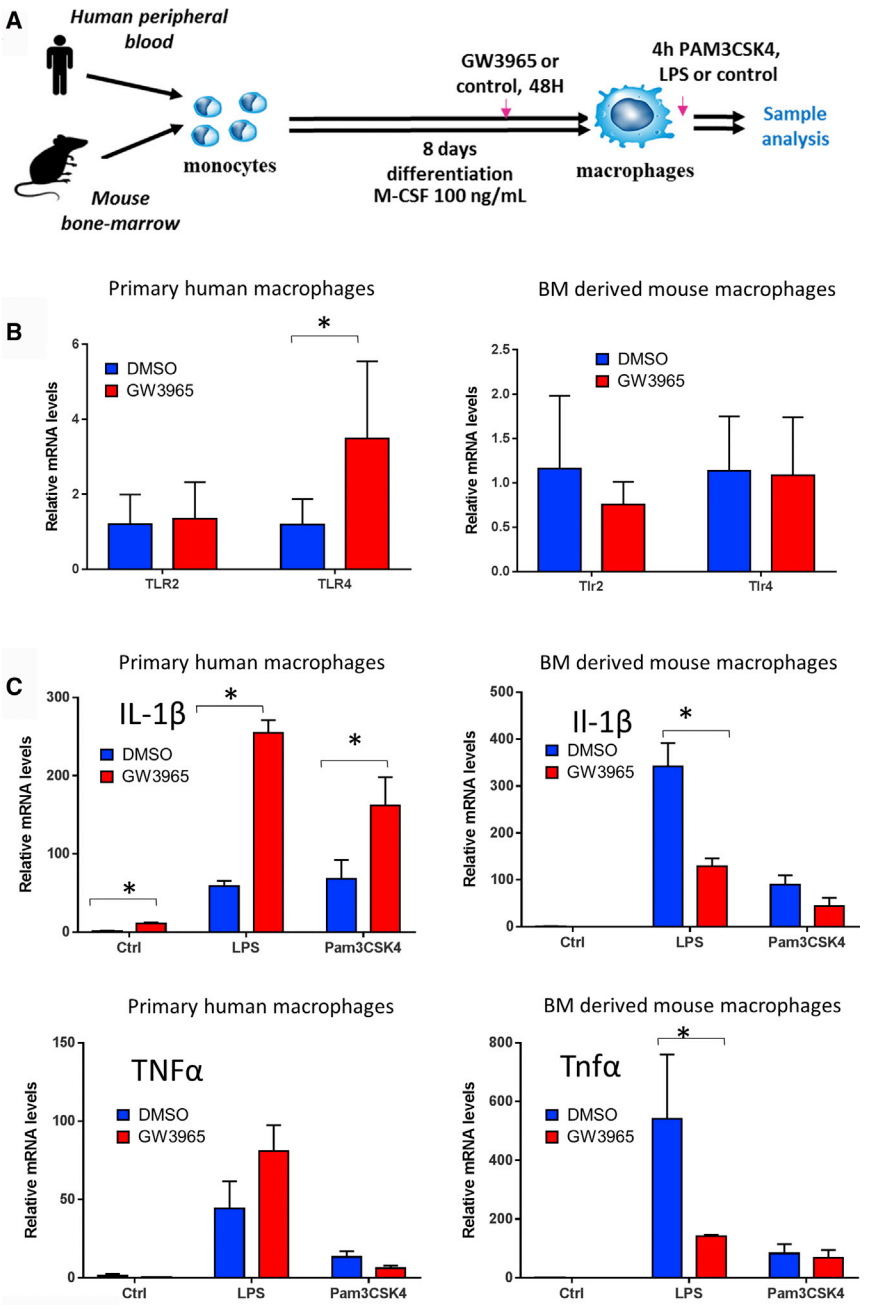

Figure 1. LXR Activation Differentially Affects TLRs Expression and Cytokine Response in Human and Mouse Macrophages

(A) General strategy used for macrophage differentiation and stimulation.

(B) Relative mRNA levels of *TLR2* and *TLR4* 48 h after GW3965 treatment without TLR activation. *p < 0.05 versus DMSO (Student's t test). n = 6 independent human donors or n = 4 independent animals.

(C) Relative mRNA levels of *IL1B* and *TNFα* 4 h after LPS or Pam3CSK4 stimulation.*p < 0.05 versus DMSO (Student's t test).

Data are representative of three independent experiments with different human donors or animals. Data are expressed as mean ± SD. See also Figure S1.

et al., 2007). It was also suggested that the anti-inflammatory activity of LXRs is related to their ability to inhibit TLR/Myd88 signaling through ABCA1-dependent cholesterol depletion of lipid rafts (Ito et al., 2015). Finally, a recent study produced evidence that LXR suppresses inflammation through *cis* repression of target genes and cholesterol efflux (Thomas et al., 2018). Although the anti-inflammatory effects of LXRs have been demonstrated mainly in mice, the paradigm in human cells is more complex (Töröcsik et al., 2010; Fontaine et al., 2007). Indeed, the lipopolysaccharide (LPS) receptor TLR4 is a LXR target in human but not in murine macrophages (Fontaine et al., 2007). As a consequence, although the anti-inflammatory potential of LXRs can be preserved to some extent in human macrophages (Spann et al., 2012), long-term exposure of human macrophages to LXR agonists leads to potentiation of the LPS response (Fontaine et al., 2007). Beyond TLR4, the modulation of other inflammatory pathways by LXRs in human macrophages remains to be explored. Particularly, TLR2 is endowed with a predominant role in triggering inflammation in the atheroma plaque (Monaco et al., 2009). Therefore, we aimed to investigate the impact of LXRs on the inflammatory response of human and murine primary macrophages stimulated by TLR4 and TLR2 agonists, with a specific emphasis on IL-1β expression in the context of human atherosclerosis.

RESULTS

LXR Activation Increases IL-1β Expression in Human Primary Macrophages Stimulated by a TLR2 Agonist

Murine bone marrow-derived macrophages (mBMDMs) and human monocyte-derived macrophages (hMDMs) were differentiated in parallel for 8 days in the presence of M-CSF (macrophage colony-stimulating factor), a standard protocol to obtain fully differentiated macrophages (Figure 1A). By using public data from previous publications using similar differentiation protocols for human and murine macrophages, we compared chromatin accessibility (assay for transposase-accessible chromatin using sequencing [ATAC-seq]) and chromatin acetylation (H3K27ac) between human and mouse macrophages at the *IL1B* locus under basal or TLR4-stimulated conditions (GEO: GSE100380, GSE85245, GSE109998, GSE95712; Park et al., 2017;

Novakovic et al., 2016; Thomas et al., 2018; Oishi et al., 2017). As shown in Figure S1A, both human and mouse macrophages display similarly low levels of chromatin acetylation and accessibility that are dramatically enhanced upon TLR4 activation. In both cases, *IL1B* mRNA levels decreased during the *in vitro* differentiation protocol (Figure S1B).

After 6 days of differentiation, macrophages were treated with GW3965, a specific LXR agonist, at 1 μM (Figure 1A). Expression of TLR2 and TLR4 was assessed at the end of the differentiation period. As previously described, LXR agonist treatment induces a significant increase in *TLR4* mRNA levels in hMDMs but not in mBMDMs (Figure 1B). In contrast, *TLR2* mRNA levels remained unchanged after LXR agonist treatment in both human and murine macrophages (Figure 1B).

Differentiated macrophages were activated by TLR4 (LPS) and TLR2 (Pam3CSK4) agonists, and the inflammatory response was assessed at the transcriptional level 4 h after TLR activation (Figure 1A) by measuring *IL1B* and *TNFα* mRNA levels. As previously described, LXR agonist pre-treatment exerts a pronounced anti-inflammatory effect in murine macrophages and inhibits both IL-1β and TNF-α response in LPS-stimulated macrophages. A similar observation was made with Pam3CSK4 but to a lesser extent (Figure 1C). As expected, GW3965 treatment potentiated the LPS response of human macrophages, with significant increases in *IL1B* and *TNFα* mRNA levels, likely due to LXR-mediated TLR4 induction. The most interesting observations came from LXR agonist-conditioned human macrophages stimulated with Pam3CSK4, with opposite effects of LXR activation on the TNF-α and IL-1β responses. Although *TNFα* mRNA levels tended to be decreased by LXR agonist pre-treatment, *IL1B* mRNA levels were robustly induced in LXR agonist-treated macrophages (Figure 1C). A similar effect of LXR activation on IL-1β was also observed with classically activated macrophages differentiated in the presence of granulocyte-macrophage colony-stimulating factor (GM-CSF) (Figure S1C), whereas no impact of LXR agonist was observed on *IL1B* mRNA levels in THP-1 cells, a widely used human monocytic cell line (Figure S1C).

IL-1β Induction by LXR Is Selective and Independent of TLR2 Activation

To further explore the mechanisms leading to the induction of *IL1B* gene expression by LXR agonist conditioning, primary human macrophages from eight donors were differentiated as described in Figure 1A. The effect of LXR agonist on *IL1B* gene expression was measured in the basal state or after exposure to Pam3CSK4. As shown in Figure 2A, in seven of eight donors, 48 h conditioning with LXR agonist induces a significant increase in *IL1B* mRNA levels in the absence of any TLR activation. A similar impact of LXR treatment was also observed in macrophages stimulated with Pam3CSK4 (Figure 2B). Although the *IL1B* mRNA levels were considerably lower in control macrophages, the magnitude of IL-1β induction by LXR agonist treatment was broadly similar in control and Pam3CSK4-treated cells. In other words, our data suggest that LXR agonists do not affect TLR2 signaling pathways but rather selectively upregulate *IL1B* gene expression. In agreement with this assumption, no impact of LXR activation was observed on the gene expression of the inflammatory cytokines *TNFα*, *IL6*, or *MCP1* (Figure S2), while a typical LXR target such as LXR-α (*NR1H3*) was consistently induced (Figure S2). Indeed, LXR activation instead resulted in the inhibition of *TNFα* gene expression (Figure S2). We also investigated the impact of shorter exposure of macrophages to LXR ligands. Six hours of conditioning with GW3965 did not result in significant changes in IL-1β expression both at the basal level and upon Pam3CSK4 activation. In contrast, with 24 h exposure, there was a significant upregulation of *IL1B* gene expression in LXR agonist-treated samples at the basal level, with a non-significant tendency ($p = 0.13$) upon Pam3CSK4 stimulation (Figure S3A).

As expected, activation of LXR with steroidal (22R-OH cholesterol) or other synthetic LXR agonists (T0901317) for 48 h triggered a rise in *IL1B* mRNA levels but not in *TNFα* mRNA levels (Figures 2C and S3B). In contrast, LXR inhibition with small interfering RNA (siRNA) targeting LXR-α, the major LXR isoform in human macrophages (Figure S3D), or with GSK2033, a synthetic LXR antagonist (Zuercher et al., 2010), abolished the induction of IL-1β mediated by GW3965 pre-treatment (Figures 2D and 2E). However, we observed that siRNA transfection reagent activated the macrophages that subsequently over-responded to TLR agonist stimulation. Consequently, the relative effect of the LXR ligand on *IL1B* in transfected cells was less pronounced. Alternatively, the lower efficiency of LXR-α siRNA to lower IL-1β expression compared with GSK2033 may be due to the presence of LXR-β (NR1H2) that is expressed at low but significant levels in human macrophages (Ishibashi et al., 2013). Again, no induction was observed with TNF-α (Figures S3C–S3E).

Importantly, changes in *IL1B* mRNA levels translated into an increase in the pro-IL-1β protein levels in LXR agonist-conditioned Pam3CSK4-stimulated cells (Figure 2F). Of note, pro-IL-1β was not detected without Pam3CSK4 stimulation. Caspase-1 expression was not affected by LXR agonist treatment (Figure S3F), and as previously described, in the absence of inflammasome activation, mature IL-1β was secreted only at very low levels in the extracellular medium by human macrophages (Figure 2G; Figure S3G). In contrast, exposure to ATP markedly induced the extracellular release of mature IL-1β. Strikingly, this event was drastically enhanced upon LXR conditioning (Figure 2G). No impact of LXR stimulation was observed for TNF-α and IL-6 secretion (Figure S3G). Thus, these data demonstrated that the induction of IL-1β by LXRs at the transcriptional level translated into increased secretion of mature IL-1β by human macrophages following TLR stimulation and inflammasome activation by ATP.

LXR-HIF-1α Pathway Drives IL-1β Induction

We sought to identify the factors potentially involved in the differential regulation of TNF-α and IL-1β by LXRs and to explain the discrepancies between murine and human macrophages. We turned our attention to the transcription factor HIF-1α. Indeed, IL-1β is a HIF-1α target (Zhang et al., 2006), and it has been shown that HIF-1α contributes to the LPS-mediated induction of IL-1β in macrophages but has no impact on TNF-α expression (Tannahill et al., 2013). Moreover, LXR and HIF-1α have been shown to cooperate to promote lipogenesis in macrophages (Na et al., 2011). Interestingly, a first transcriptional approach

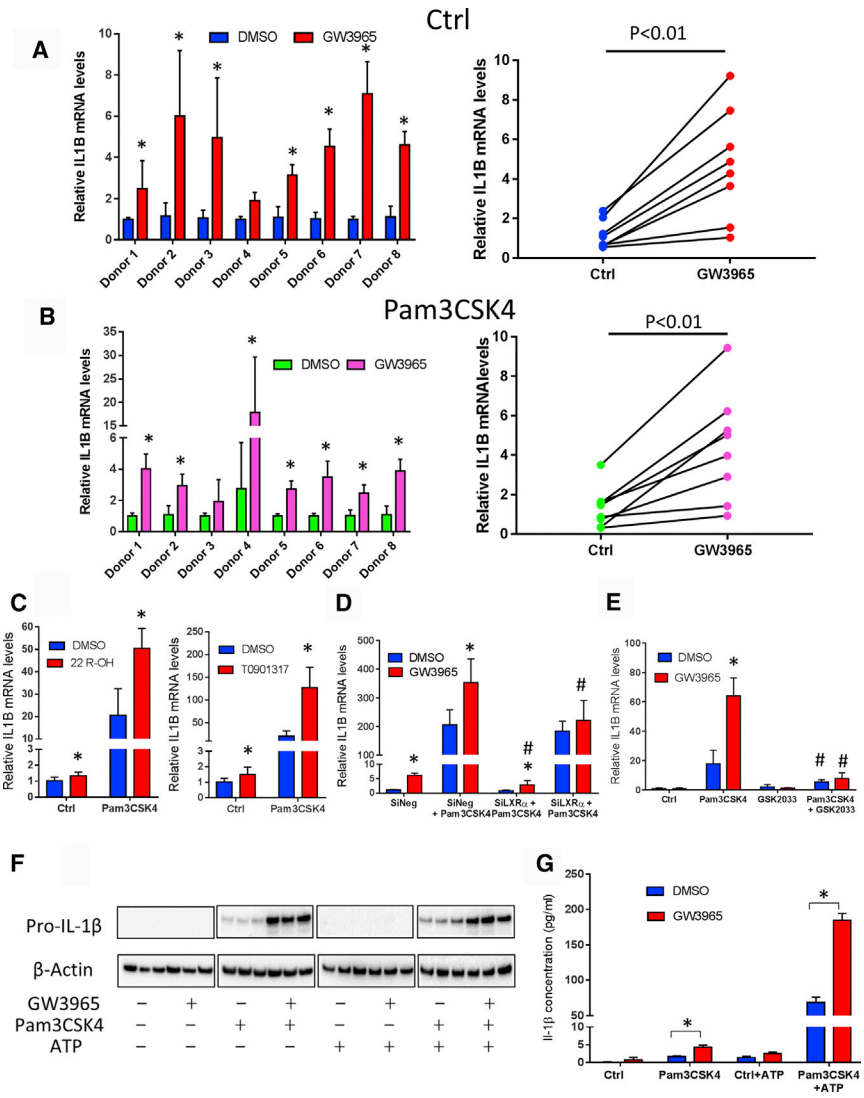

Figure 2. LXR Activation Increases IL-1β Production in Human Macrophages

(A) *IL1B* mRNA levels in unstimulated macrophages treated or not with GW3965 for 48 h. In the left panel, data are normalized at 1 for each donor in the DMSO conditions. *p < 0.05 versus DMSO (Student's t test). In the right panel, relative expression levels are calculated for each donor. *p < 0.01 (paired t test).

(B) *IL1B* mRNA levels 4 h after Pam3CSK4 stimulation; same representation.

(C) Relative *IL1B* mRNA levels in macrophages treated with different LXR agonists. *p < 0.05 versus DMSO (same stimulation conditions, two-way ANOVA, Sidak's test).

(D) Relative *IL1B* mRNA levels in macrophages treated with negative or LXR-α SiRNA. *p < 0.05 versus DMSO (same stimulation conditions), #p < 0.05 versus SiNeg (same treatment and stimulation conditions, two-way ANOVA, Sidak's test). Data are representative of three independent experiments with individual donors.

(E) Relative *IL1B* mRNA levels in macrophages treated with DMSO or the LXR antagonist GSK2033. *p < 0.05 versus DMSO (same stimulation conditions), #p < 0.05 versus no LXR antagonist (same treatment and stimulation conditions, two-way ANOVA, Sidak's test). Data are representative of three independent experiments with individual donors.

(F) Pro-IL-1β protein levels analyzed using western blot. β actin is used as loading control. Macrophages were differentiated and treated with GW3965 and/or Pam3CSK4 as described above and then stimulated or not with ATP (3 mM) for 45 min before analysis.

(G) IL-1β concentration in cell supernatants determined using ELISA. *p < 0.05 versus DMSO (Student's t test).

Data are representative of three independent donors. Data are expressed as mean ± SD. See also Figures S2 and S3.

revealed that *HIF1α* mRNA levels were increased after LXR agonist treatment of human macrophages at the basal state level as well as in combination with Pam3CSK4 (Figures 3A and 3B). As expected, TLR2 agonist induced an increase in *HIF1α* mRNA levels in control and LXR-treated macrophages (Figure 3A). At the protein level, these observations were confirmed by ELISA (Figure 3D). Importantly, LXR-mediated induction of *HIF1α* mRNA levels was absent in mBMDMs (Figure 3C). Higher nuclear and cytoplasmic HIF-1α staining was observed by immunofluorescence analysis in LXR- and/or Pam3CSK4-treated human macrophages compared with control macrophages (Figure 3E). In contrast, no LXR agonist-mediated change was observed in murine macrophages where Pam3CSK4 slightly increases HIF-1α staining, as expected (Figure S4A).

To determine whether HIF-1α was involved in the LXR-mediated induction of *IL1B* gene expression, we neutralized HIF-1α with either a pharmacological inhibitor (FM19G11) (Moreno-Manzano et al., 2010) or siRNAs. FM19G11 has been shown to prevent HIF-1α protein accumulation in cells during hypoxia and to decrease HIF-1α occupancy to the promoter of target genes (Moreno-Manzano et al., 2010). In both cases, HIF-1α inhibition abolished the impact of LXR on IL-1β expression (Figures 3F, 3G, and S4B). Thus, our data demonstrate that LXR-mediated HIF-1α induction is required for the increase in *IL1B* mRNA levels.

Several Pathways Promote HIF-1α and IL-1β Induction

To further confirm the role of the LXR/HIF1a axis in the transcriptional regulation of *IL1B*, we explored potential HIF-1α-dependent epigenetic changes in *IL1B* gene promoter. Histone 3 (H3) acetylation around the hypoxia-responsive element (HRE) of the *IL1B* promoter was assessed using chromatin immunoprecipitation (ChIP). In line with our hypothesis, a significant enrichment in H3 acetylation was observed after the exposure of

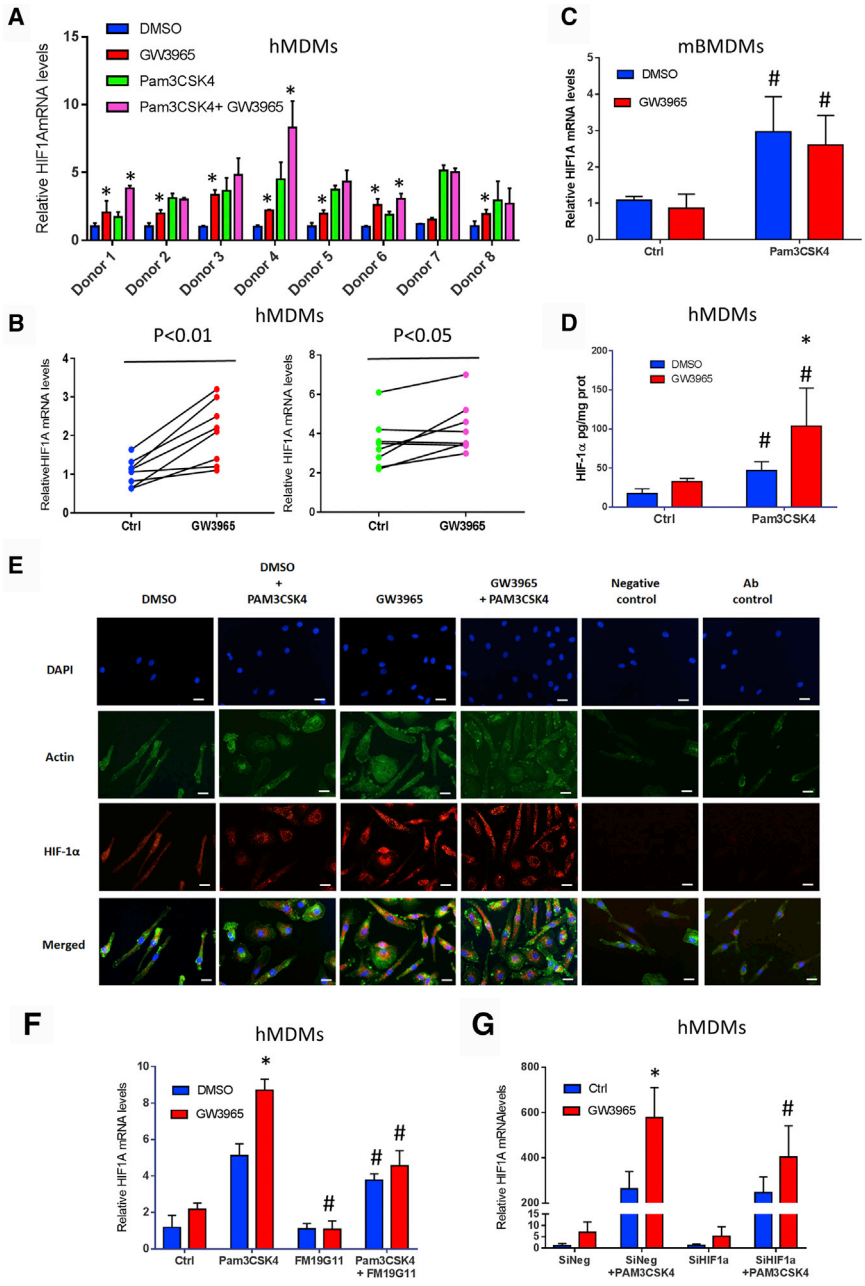

Figure 3. LXR-Mediated HIF-1α Induction Increases IL-1β Expression

(A) *HIF1α* mRNA levels. Human macrophages were treated or not with GW3965 at 1 μM for 48 h and stimulated with Pam3CSK4 or a control treatment for 4 h. *p < 0.05 versus DMSO (same stimulation conditions, Student's t test).

(B) Relative expression levels are calculated for each donor (paired t test).

(C) *Hif1α* mRNA levels. Mouse bone marrow-derived macrophages were treated or not with GW3965 at 1 μM for 48 h and were stimulated with Pam3CSK4 or a control treatment for 4 h. #p < 0.05 versus unstimulated macrophages with same LXR agonist or DMSO treatment (two-way ANOVA, Sidak's test). n = 3 independent mice.

(D) HIF-1α protein concentration in cell lysates. Human macrophages were treated as described above, and HIF-1α protein levels were determined using ELISA. *p < 0.05 versus DMSO (same stimulation conditions), #p < 0.05 versus unstimulated macrophages with same LXR agonist or DMSO treatment (two-way ANOVA, Sidak's test). n = 3 independent donors.

(E) Representative immunostaining of HIF-1α (red). Nuclei are stained with DAPI and F-actin with phalloidin (green). Human macrophages were differentiated and treated as describe in (A). Scale bar, 5 μm.

(F) Relative *IL1B* mRNA levels in macrophages treated with DMSO or the HIF-1α inhibitor FM19G11. *p < 0.05 versus DMSO (same stimulation conditions), #p < 0.05 versus no HIF-1α inhibitor (same treatment and stimulation conditions, two-way ANOVA, Sidak's test). Data are representative of two independent experiments with distinct donors.

(G) Relative *IL1B* mRNA levels in macrophages treated with negative or *HIF1α* siRNA. Human macrophages were differentiated and treated as describe in (A). *p < 0.05 versus DMSO (same stimulation conditions), #p < 0.05 versus SiNeg (same treatment and same stimulation conditions, two-way ANOVA, Sidak's test).

Data are expressed as mean ± SD. Data are representative of three independent experiments with individual donors. See also Figure S4.

human macrophages to an LXR agonist (Figure 4A), further supporting the implication of HIF-1α in *IL1B* induction.

LXR agonists activate both the *HIF1α* and *IL1B* genes, and *HIF1α* is also endowed with an HRE in its own promoter (Koslowski et al., 2011); therefore we analyzed the recruitment of HIF-1α and LXR-α to the promoter of these two genes. We could only validate a ChIP experiment for HIF-1α for one individual donor that confirmed a significant HIF-1α occupancy at the previously described HREs on the *IL1B* and *HIF1α* gene promoters. Although quantification was difficult because of high background and technical variability, promoter occupancy by HIF-1α did not seem to be altered by GW3965 treatment (data not shown). Unexpectedly, although no significant LXR-α binding could be observed in DMSO-treated samples, we observed that GW3965 treatment resulted in a significant binding of LXR-α at the two HRE sites on *IL1B* and *HIF1α* gene promoters, but at a lower magnitude compared with a typical LXRE such as the one present in the *NR1H3* promoter (Figure 4B). Although the present study does not demonstrate a direct interaction between LXR-α/HIF-1α, our data support the existence of LXR-α/HIF-1α complexes on *HIF1α* and *IL1B* promoters upon LXR activation, which would provide a potential mechanism to explain both *IL1B* and *HIF1α* induction.

In parallel, we explored the potential implication of other pathways that are known to modulate *HIF1α* gene expression. In particular, HIF-1α is known to be regulated by reactive oxygen

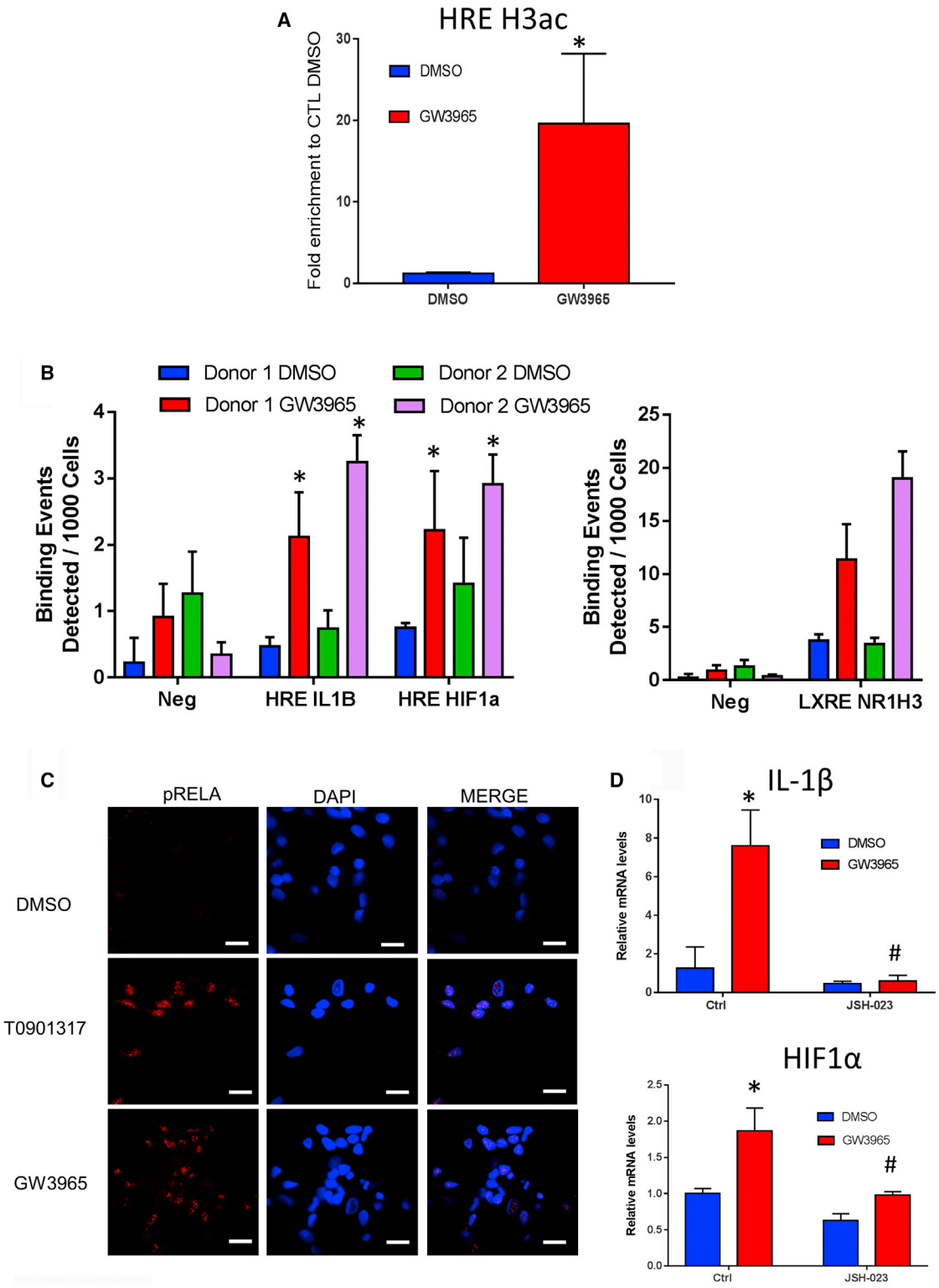

Figure 4. Several Pathways Promotes HIF-1α and IL-1β Induction

(A) Relative enrichment in histone 3 acetylation near hypoxia-responsive element of the *IL1B* promoter was analyzed using chromatin immunoprecipitation followed by real-time PCR (ChIP-qPCR). Differentiated macrophages were treated with or without GW3965 at 1 μM for 48 h. *$p < 0.05$ versus DMSO (Student's t test).

(legend continued on next page)

species (ROS) through an NF-κB-dependent pathway (Bonello et al., 2007). As previously described, we noticed that LXR agonists increase ROS production in human but not murine macrophages (data not shown) (Fontaine et al., 2007). Therefore, in order to measure a potential activation of NF-κB, we analyzed the nuclear translocation of phospho-RELA (p65) by immunofluorescence. As shown in Figure 4C, 48 h treatment with GW3965 or T0901317 induced a slight activation of NF-κB in the absence of any TLR stimulation. Moreover, co-treatment with the pharmacological NF-κB inhibitor JSH-023 abolished the GW3965-mediated increase of *HIF1α* and *IL1B* mRNA levels (Figure 4D).

LXR Agonists Potentiate HIF-1α Signaling in Human Macrophages

LXR-mediated regulation of HIF-1α could theoretically affect other HIF-1α-regulated pathways besides IL-1β. To test this hypothesis, we reanalyzed microarray data previously published by our group (Rébé et al., 2009) of human monocytes treated for 48 h with T0901317, a potent LXR activator. In two independent donors, we observed that several HIF-1α target genes, including *IL1B*, were positively regulated by T0901317 (Figures 5A and 5B). Regulated genes were involved in angiogenesis (*VEGFA*, *CxCR4*) and glycolysis pathways (*GLUT1*, *HK2*, *PDK1*, *PFKFB3*). The microarray data were confirmed by qPCR analysis in three additional independent donors. For ten genes, including *IL1B*, *HIF1α*, *GLUT1*, *VEGFA*, and *CXCR4*, significant induction was observed (Figure 5B). By gene set enrichment analysis using Metascape, the HIF-1α-regulated pathways noted by the Gene Ontology (GO) terms "angiogenesis" and "cellular carbohydrate metabolic process" were significantly enriched by T0901317 treatment (Figure 5C). The KEGG (Kyoto Encyclopedia of Genes and Genomes) pathway "HIF1a pathway" was also significantly enriched according to DAVID (not shown). These data, obtained in human monocytes, were confirmed in GW3965-exposed human macrophages. As depicted in Figure 5D, exposure to GW3965 leads to significant increases in *GLUT1*, *HK2*, *VEGFα*, and *CxCR4* mRNA levels. GLUT1 and VEGF were previously described as LXR targets (Kase et al., 2005; Walczak et al., 2004). Here, we assessed the contribution of HIF-1α in this LXR-mediated gene regulation. Interestingly, HIF-1α knockdown significantly reduced the mRNA levels of *GLUT1*, *HK2*, *VEGFα*, and *CxCR4* in LXR agonist-treated cells, whereas it had almost no effect in control cells. This suggests that HIF-1α substantially contributed to the LXR-mediated induction of these genes (Figure 5E). An opposite picture was observed in mBMDMs, in which LXR-mediated increase of glycolysis genes was absent (Figure S5A). This further strengthens the differential response between human and murine macrophages. Finally, we measured the glycolytic activity of human and murine macrophages stimulated with Pam3CSK4 in combination with GW3965 or not (Figures 5F and 5G; Figure S5B). At basal settings, human macrophages display a low glycolytic rate. Pam3CSK4, GW3965, or GW3965/Pam3CSK4 sequential stimulation markedly induced it. Although the induction of glycolysis following TLR agonist stimulation was quite expected, our results indicate that LXR activation promotes glycolysis in primary human macrophages. The picture was very different in mouse macrophages. Indeed, although TLR2 agonist promoted, as expected, a marked increase in the glycolytic activity of macrophages, GW3965 treatment strongly inhibited glycolysis either in control or in Pam3CSK4-treated cells (Figure 5G; Figure S5B).

Human Carotid Plaque Samples Increase IL-1β Expression in an LXR-Dependent Manner

Human atherosclerotic plaques contain a complex mixture of oxidized lipids, such as oxysterols, fatty acids, and retinoids, which are able to activate, among other pathways, the LXR/RXR axis (Rébé et al., 2009). In order to mimic the settings of the plaque, human primary macrophages were exposed to homogenates prepared from human atheroma plaques. Plaque homogenates were added to the culture medium at 1:100, and they were incubated for 48 h with macrophages with or without the LXR antagonist GSK2033. After 48 h incubation, all plaque debris were phagocytized by macrophages which acquired a foamy morphology (Figure S6A). As previously reported (Rébé et al., 2009), plaque homogenates markedly induced LXR-regulated genes, including ABCA1 and ABCG1 (Figure 6A; Figure S6C). This induction was significantly attenuated in the presence of GSK2033, a selective LXR antagonist (Figure 6A). Strikingly, plaque homogenates markedly induced the gene expression of *IL1B* compared with control samples. Again, this effect was blunted by GSK2033, further supporting the involvement of LXR signaling (Figure 6A). Interestingly, plaque homogenates also slightly induced *HIF1α* mRNA levels (Figure 6A), and *HIF1α* mRNA levels strongly correlated with the induction of *IL1B* gene expression (Figure S6B). In contrast, healthy carotid samples had no impact on *IL1B* mRNA levels (Figure S6D). Interestingly, although 48 h exposure to plaques samples did not affect *TNFα* mRNA levels, GSK2033 weakly induced *TNFα* in macrophages exposed to plaque homogenates (Figure S6C). Preincubation of macrophages with plaque homogenates from the same donors also potentiated IL-1β response following TLR2 stimulation but did not induce TNF-α (Figure 6B; Figure S6E).

To confirm our results with an unbiased approach, we performed a whole-transcriptome analysis by using RNA

(B) ChIP-qPCR was used to analyze the recruitment of LXR-α onto the promoter regions of *IL1B* and *HIF1a* containing hypoxia-responsive elements. Differentiated macrophages were treated as described above. The presence of DNA regions of interest was analyzed using qPCR using the immunoprecipitated DNA. Negative control amplifies a region in a gene desert where transcription factor binding is not expected to occur. *$p < 0.05$ versus negative control (same donor and conditions, Student's t test).

(C) Primary macrophages were treated with GW3965 or T0901317 at 1 μM for 48 h, phospho-RELA (p65) phosphorylation (pS536) was assessed by confocal microscopy. Scale bar: 5 μm.

(D) Differentiated macrophages were treated with GW3965 at 1 μM with or without JSH-023 at 30 μM for 48 h. *$p < 0.05$ versus DMSO (same stimulation conditions), #$p < 0.05$ versus without JSH-023 (same LXR treatment, two-way ANOVA, Sidak's test).

Data are expressed as mean ± SD. Data are representative of two independent experiments with distinct donors.

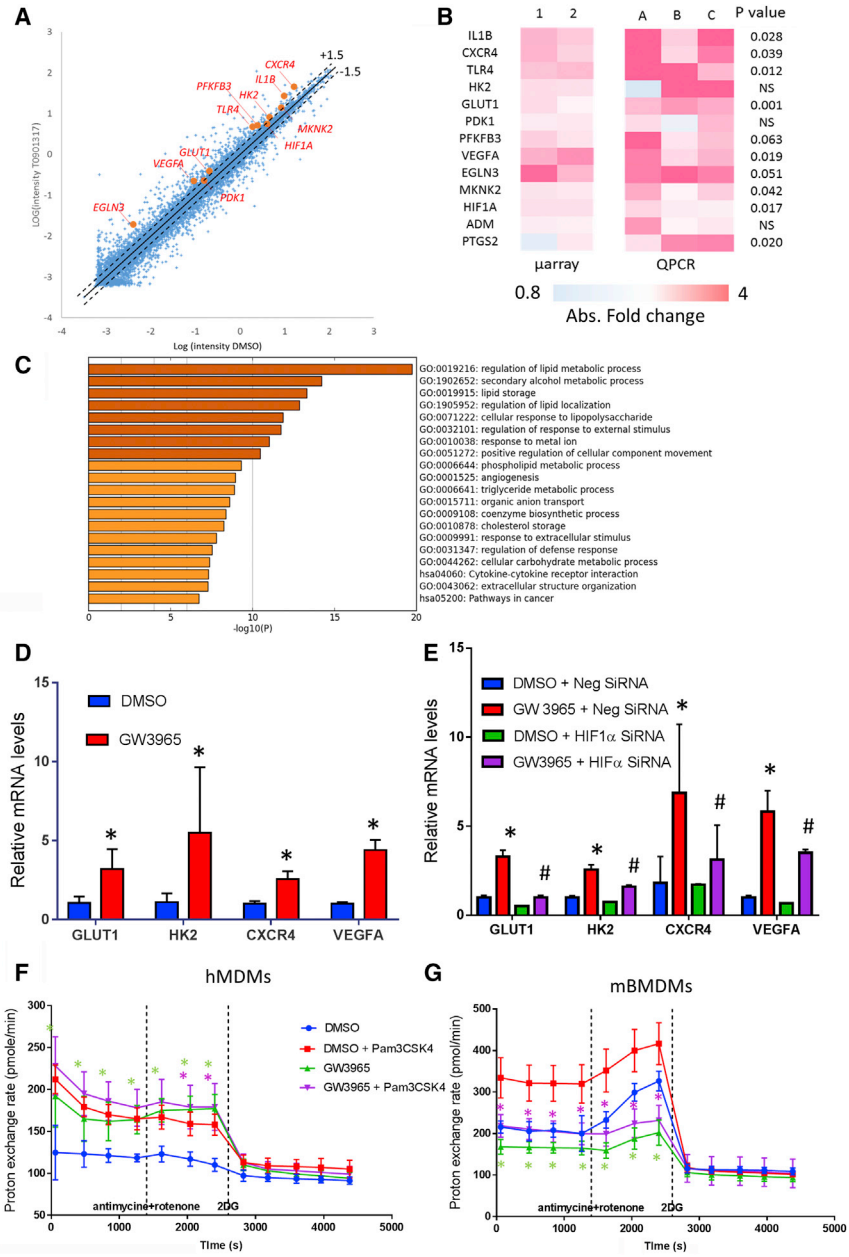

Figure 5. LXRs Activate Other HIF-1α-Dependent Pathways

(A) Representative scatterplots for up- and down-regulated genes analyzed using microarray in human monocytes treated with T0901317 (10 μM) for 48 h. Representative HIF-1α target genes are highlighted in red. Dotted lines represent ±1.5-fold changes compared with DMSO-treated cells.

(B) Heatmap for key HIF-1α target genes compared with DMSO-treated monocytes from two independent donors (microarray data) and three additional independent donors (qPCR data). Student's t test.

(C) GO term analysis of upregulated genes in primary human monocytes according to Metascape analysis of the microarray experiment.

(D) mRNA levels of HIF-1α target genes in primary human macrophages treated or not for 48 h with GW3965 at 1 μM. *p < 0.05 versus DMSO (Student's t test). n = 3 independent donors.

(E) mRNA levels of HIF-1α target genes in Pam3CSK4-stimulated human macrophages transfected with negative or HIF-1α SiRNA. *p < 0.05 versus DMSO (same stimulation conditions), #p < 0.05 versus no HIF-1α inhibitor (same treatment and stimulation conditions, two-way ANOVA, Sidak's test). Data are representative of two independent experiments with distinct donors.

(F) Proton exchange rate recording of human and mouse macrophages treated as described above. *p < 0.05 versus DMSO (same stimulation conditions, two-way ANOVA, Sidak's test).

Data are expressed as mean ± SD. Data are representative of three independent donors or animals. See also Figure S5.

sequencing of human macrophages incubated with plaque samples from three additional distinct donors for 48 h with or without GSK2033. Plaque treatment resulted in the significant induction of 426 genes, among which LXR targets such as *ABCA1*, *ABCG1*, *RARA*, and *CD82* were highly induced (Figures 6C and 6D). *NR1H3* was also significantly induced (adjusted p < 0.00019). Importantly, *IL1B* was among the 100 most induced genes. Gene set enrichment analysis revealed that the major pathways enriched were involved in cell migration, cellular response to LPS, and lipids (Figure 6C). The *HIF1α* pathway was also significantly enriched (Figure 6C) with *HIF1α* target genes involved in glycolysis such as *HK2*, *HK3*, and *SLC2A1*. As expected, genes involved in cholesterol synthesis were markedly downregulated by treatment with plaque samples (Figures S7A and S7B). Combined exposure of macrophages to atheroma plaque samples and GSK2033 had a limited impact compared with plaque exposure alone, with 56 transcripts downregulated and 7 transcripts upregulated (Figures 6D and S7B). Interestingly, *ABCG1*, *ABCA1*, and *IL1B* were present among the 29 genes that were significantly induced by plaque exposure and inhibited by GSK2033 (Figures 6D and 6E). Intriguingly, IL-18BP, an inhibitor of IL-18 and a recently described LXR target (Pourcet et al., 2016) was among the two genes inhibited by plaque samples and upregulated by GSK2033.

We characterized 27 plaques samples using a targeted lipidomic analysis of sterols. Clinical parameters of patients are given in Table S1. As expected, samples contained high amounts of cholesterol and oxidized sterols, notably 27-OH cholesterol (Figures 7A and S8A). Individual and total oxysterol content of the plaques (including 27-OH, 25-OH, 7-alpha-, 7-beta-, and 7-oxo-cholesterol but not 24-OH cholesterol or desmosterol) strongly correlated with the ability of plaques homogenates to induce IL-1β from primary macrophages (Figures 7B and S8B), while cholesterol content did not reach statistical significance

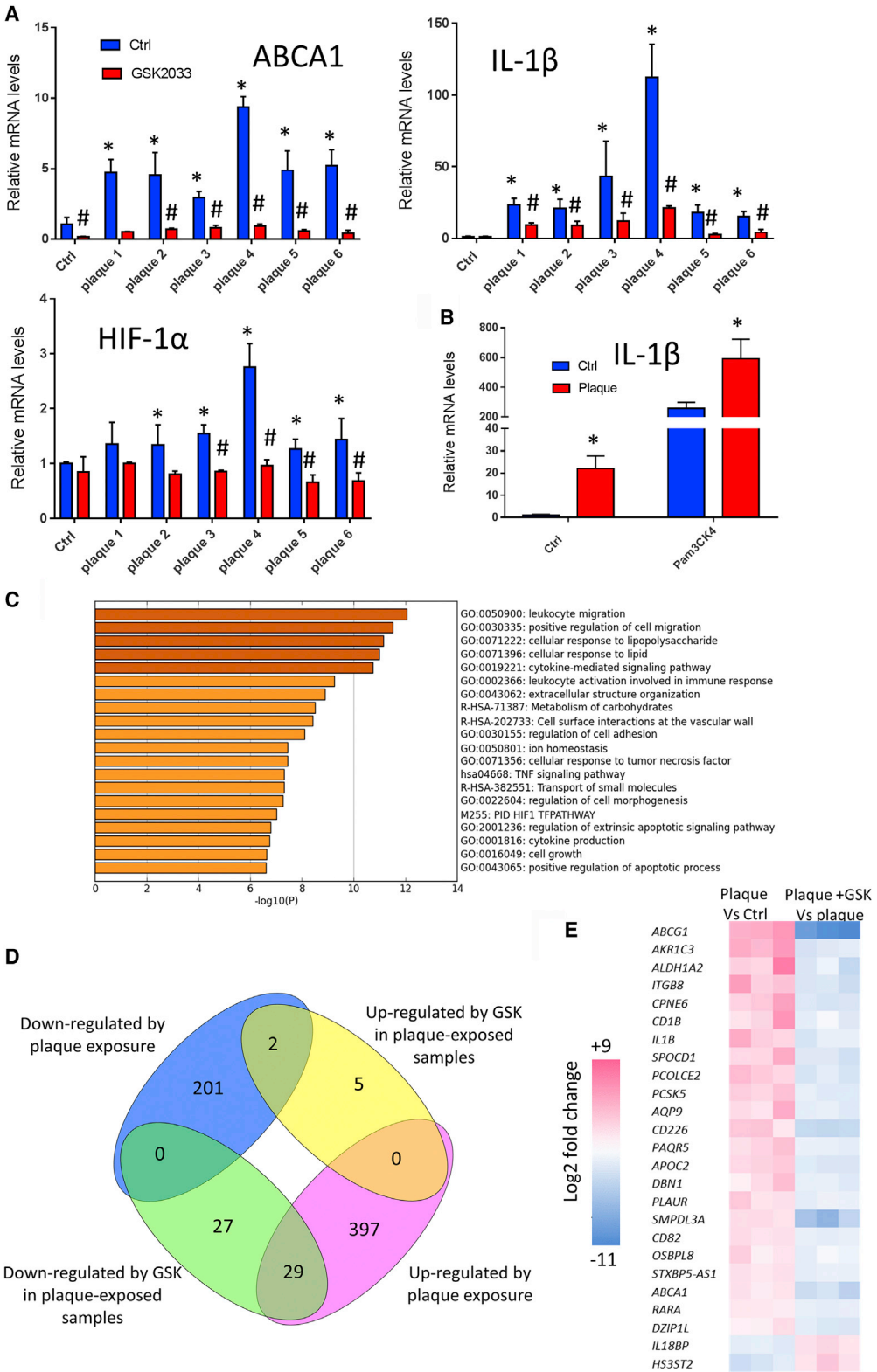

(legend on next page)

(Figure S8B). For some oxysterol (including 7-beta- and 25 OH cholesterol), there was also a correlation with the ability of plaque extract to induce the cholesterol transporter ABCG1. For ABCA1, correlations were weaker, possibly related to the lower magnitude of induction; nevertheless the desmosterol content tended to correlate with the ability of plaque homogenates to increase *ABCA1* mRNA levels (Figure S8) a tendency that was not observed for IL-1β and ABCG1.

IL-1β Colocalizes with HIF-1α and LXR-α in Macrophage-Rich Areas of Human Carotid Artery Plaques

We examined the localization of HIF-1α and LXR-α in human atheroma plaques using immunohistochemistry. All the plaque samples were strongly positive for LXR-α. LXR staining was observed mainly in the nuclei of the cells and was localized predominantly in macrophage-enriched areas, as assessed by CD68 staining (Figure 7C). Six of seven plaque samples were positive for HIF-1α. HIF-1α also displayed a predominant localization in macrophage-enriched areas, even though it was more restricted than LXR (Figure 7C). Interestingly, IL-1β was also detected in these LXR-α/HIF-1α-positive regions. In contrast, neither HIF-1α nor IL-1β staining was observed in healthy areas of the arteries, while LXR-α and CD68 staining was limited to a very small number of positive cells (Figure S9). Co-localization studies by using immunofluorescence approaches were also performed for LXR-α and HIF-α and for LXR-α and CD68, respectively (Figure 7). LXR and HIF-1α display nuclear colocalization in positive cells; moreover, the majority of cells positive for LXR staining also display positive HIF-1α staining. LXR and CD68 double staining confirmed that LXR-α is expressed mainly in CD68-positive cells (Figures 7D and 7E). Overall, our results indicate that the regulation of IL-1β by the LXR-α/HIF-1α axis is likely functional in human atherosclerotic lesions.

DISCUSSION

Because of its prominent role in the development of atherosclerosis, IL-1β production within the atheroma plaque represents an interesting target. Among others, two important players stand out to promote IL-1β secretion: cholesterol accumulation and the conditions of partial hypoxia that are present in the atherosclerotic lesions (Sluimer et al., 2008; Folco et al., 2014). In particular, hypoxia seems to play a key role in the production of IL-1β; indeed, IL-1β localizes preferentially with markers of hypoxia such as HK2 and HIF-1α within human atheroma plaques (Folco et al., 2014). From a mechanistic standpoint, compared with cytokines such as TNF-α, IL-1β is a target of HIF-1α endowed with HREs in its gene promoter (Zhang et al., 2006; Tannahill et al., 2013). At the post-translational level, hypoxia increases the stability of pro-IL-1β by selectively reducing its addressing to the autophagy machinery and also contributes to the activation of the inflammasome (Folco et al., 2014). On their side, cholesterol crystals activate inflammasome and play a major role in the secretion of mature IL-1β in the context of atherosclerosis (Duewell et al., 2010). Our results gather these two pathways and provide a new mechanism by which cholesterol accumulation within the plaque induces the production of IL-1β. In a pathological perspective, this work highlights the ability of atheroma plaque homogenates to activate IL-1β in a LXR-dependent manner as well as the colocalization of LXR with HIF-1α and IL-1β in macrophage-rich regions of atheroma plaques.

An interaction between HIF-1α and LXR-α in primary human macrophages as well as RAW 264.7 cells resulting in the activation of lipogenesis and foam cell formation was reported previously (Na et al., 2011). The authors suggested that LXR-α increases HIF-1α protein stability by interacting with the oxygen-dependent degradation domain of HIF-1α. Additionally, the transcriptional regulation of HIF-1α by LXR was ruled out in that study. However, the authors did not measure *HIF1α* mRNA levels in primary human macrophages following LXR activation. Therefore, this point remains debatable. Here, we undoubtedly demonstrated a parallel increase in *HIF1α* mRNA and protein levels in human macrophages exposed to LXR agonists. Moreover, we observed that the LXR-mediated induction in HIF-1α mRNA and protein levels is present in human macrophages but not in mouse macrophages.

We did not find any obvious LXR-responsive elements in the vicinity of the *HIF1α* or *IL1B* gene, and previous ChIP sequencing (ChIP-seq) databases in THP-1 cells did not reveal LXR binding peaks near theses gene in THP-1 cells (Pehkonen et al., 2012; Feldmann et al., 2013). Nevertheless, by using a more sensitive ChIP-qPCR approach in primary human macrophages, we observed a significant LXR recruitment at the HREs that are present in the *IL1B* or *HIF1α* promoters following GW3965 exposure. However, it occurred at a lower magnitude compared with a well-characterized LXRE. Thus, although we did not demonstrate a direct interaction between HIF-1α and LXR-α, our data support the study of Na et al. (2011) describing the corecruitment of HIF-1α and LXR-α to the promoters of target genes and provide a potential explanation for the concomitant activation of *HIF1α* and *IL1B* by LXR-α.

In parallel, we explored other indirect mechanisms that could be involved in HIF-1α activation. HIF-1α is an NF-κB target, and ROS were shown to activate HIF-1α at the transcriptional level through

Figure 6. Atheroma Plaque Homogenates Activate IL-1β through an LXR-Dependent Mechanism

(A) mRNA levels of target genes in human macrophages treated with atheroma plaques homogenates with or without the LXR antagonist GSK2033 for 48 h. *p < 0.05 versus control (Ctrl), #p < 0.05 versus no GSK2033 (same plaque samples, two-way ANOVA, Fisher's exact test).

(B) *IL1B* mRNA levels in human macrophages treated for 48 h with or without plaque homogenates before and after Pam3CSK4 activation (4 h). *p < 0.05 versus without plaque extract.

(C) GO term analysis of upregulated genes after 48 h exposure to plaques homogenates according to Metascape analysis of RNA sequencing data.

(D) Venn diagram of differentially expressed genes in plaque-exposed group versus plaque + GSK exposed group from RNA sequencing data.

(E) Heatmap of differentially expressed genes from RNA sequencing data in plaque-exposed group versus plaque + GSK2033. Only differentially expressed genes in both conditions (plaque versus control and plaque + GSK versus plaque) are shown.

Data are expressed as mean ± SD. See also Figures S6 and S7.

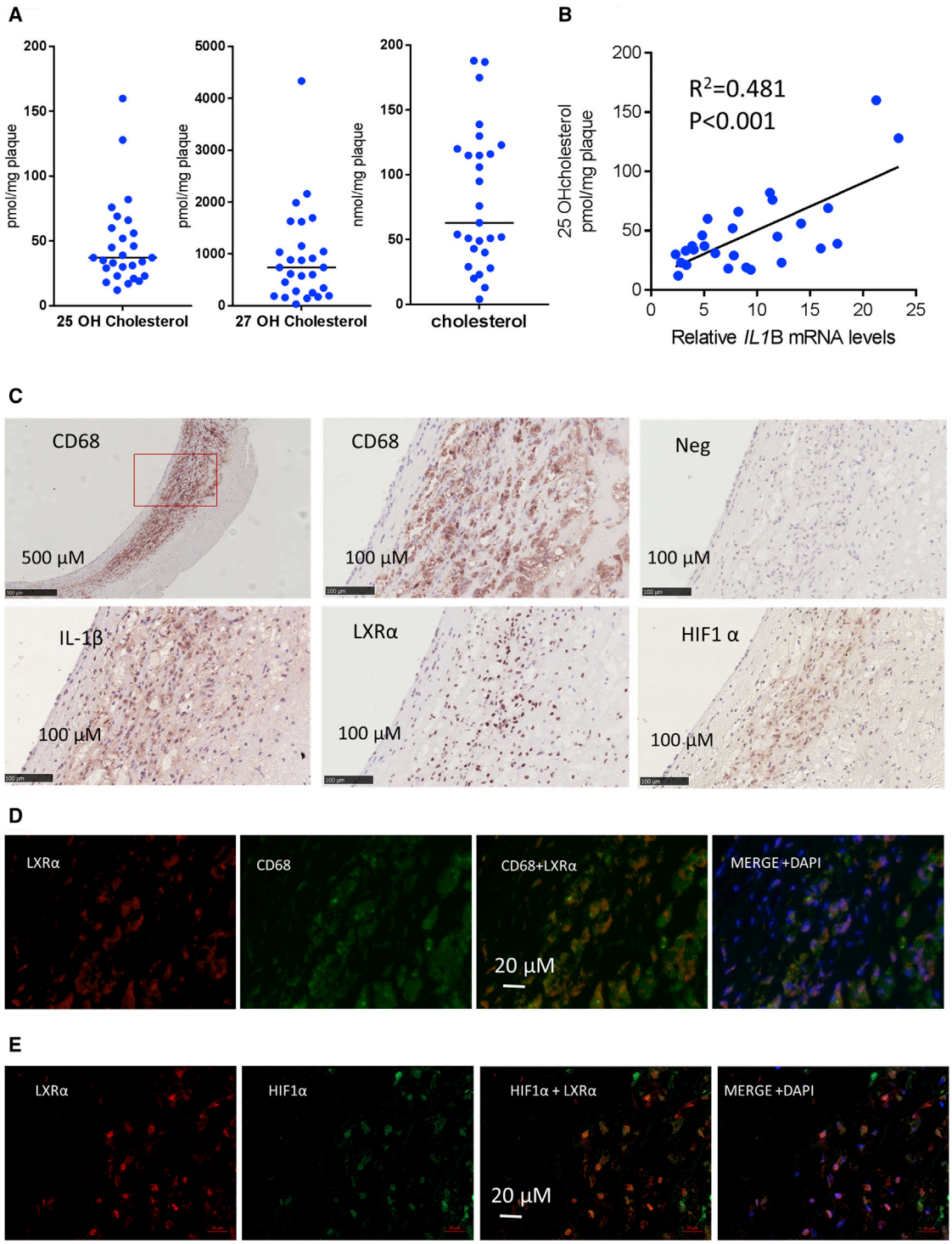

Figure 7. Oxysterol Content of Plaques Correlates with IL-1β Induction, and LXR-α and HIF-1α Colocalize with IL-1β in Macrophage-Rich Areas of Human Atherosclerotic Lesions from Carotid Arteries

(A) Oxysterol content in human atheroma plaques (data are expressed as nmol/mg or pmol/mg of tissue).

(B) Correlation between 25-OH cholesterol levels and *IL1B* mRNA levels in primary human macrophages treated with same plaques homogenates. Pearson, two tailed, Bonferroni correction for multiple comparison.

(legend continued on next page)

an NF-κB-dependent pathway (Bonello et al., 2007). Although ROS have both inhibitory or stimulatory actions on NF-κB, they have been shown to activate NF-κB through different mechanisms, including alternative IκBα phosphorylation or by increasing RelA phosphorylation (Morgan and Liu, 2011). Interestingly, LXR agonists increase ROS production in human but not in mouse macrophages, in tandem with the induction of membrane NADPH oxidase activity (Fontaine et al., 2007). We observe here that 48 h incubation with LXR agonist induces a constitutive activation of NF-κB in human macrophages. Moreover, a pharmacological NF-κB inhibitor abolishes the LXR-mediated induction of *HIF1α* and *IL1B* mRNA levels, thus demonstrating the requirement of this pathway for the regulation of IL-1β by LXR.

Importantly, our results demonstrate that the LXR/HIF-1α axis is not restricted to IL-1β. Indeed, other HIF-1α-dependent metabolic pathways are significantly activated by LXR and display similar human selectivity. Genes involved in glycolysis such as *GLUT1* and *HK2* are strongly induced by LXR in a HIF-1α-dependent manner in human macrophages, whereas LXR activation has almost no impact in murine macrophages. Interestingly, a similar pattern was recently reported in human versus murine macrophages exposed to steroidal and non-steroidal LXR agonists (Muse et al., 2018). Nevertheless, the present study reveals a fundamental difference between human and murine macrophages regarding the metabolic response to LXR activation. This work stresses that LXR agonists induce an opposite metabolic switch in human and murine macrophages, with a marked induction of glycolysis in human macrophages following LXR activation. It is established that some macrophage subpopulations present within the atheroma plaque display high glucose uptake activity. Nevertheless, the molecular mechanisms as well as the pathophysiological significance of this high glucose influx remain unclear (Sarrazy et al., 2016; Folco et al., 2011; Nishizawa et al., 2014). Our results shed new lights on these points and suggest a potential role of LXRs and its activators (namely, cholesterol accumulation) in the control of the metabolic activity of macrophages within the atheroma plaque.

Interestingly, hypoxia and HIF-1α have been proposed as regulators of cholesterol homeostasis in macrophages in atheroma plaques. Hypoxic mouse macrophages display increased cholesterol content due in part to inhibition of ABCA1-dependent cholesterol efflux mediated by HIF-1α (Parathath et al., 2011). In contrast, in human macrophages, it has been shown that the HIF-1α complex specifically binds to an HRE present in the *ABCA1* gene promoter and increases *ABCA1* promoter activity and ABCA1 expression (Ugocsai et al., 2010). The potential interplay between HIF-1α and LXR that we observed in the present study may have important consequences for the regulation of cholesterol efflux and deserves further investigation. Although we did not directly assess cholesterol efflux in the present study, we did not observe significant changes in *ABCA1* mRNA levels upon HIF-1α inhibition (data not shown).

The impact of LXR agonists on the inflammatory response of macrophages as well as the underlying molecular mechanisms remain controversial. One of the explanations certainly lies in the differences among the models and experimental protocols used among studies. Our results mainly confirm the data in the literature, namely, anti-inflammatory activity of LXR agonists in murine macrophages that is preserved in human macrophages in the context of short-term exposure to LXR agonists. However, LXR-mediated TLR4 induction in human macrophages is associated with a potentiation of the LPS response. Now, our study brings an additional piece to this puzzle and discloses a novel mechanism linking LXR and inflammation that is independent of the TLR response. This mechanism, selective to IL-1β, does not affect the expression of other cytokines such as TNF-α.

Interestingly, the use of a synthetic LXR antagonist markedly attenuated the induction of *IL1B* mRNA levels promoted by atheroma plaque homogenates, pointing to a new pharmacological way to inhibit IL-1β production within the plaque. However, such molecules also strongly inhibit cholesterol efflux pathways and might lead to an increase in cholesterol accumulation in macrophages, which is likely to promote adverse effects in the long term (Westerterp et al., 2018). Because LXR-dependent induction of IL-1β gene seems to differ from a direct transactivation, the identification of selective LXR modulators devoid of an activating effect on IL-1β is a path that deserves further attention. Development of such molecules could be hampered by well-known side effects, such as hepatic steatosis, that have precluded the clinical use of LXR agonists despite their high therapeutic potential (Kirchgessner et al., 2016; Hong and Tontonoz, 2014).

Alternatively, the development of selective LXR antagonists inhibiting the LXR-HIF-1α axis without negative effects on LXR-cholesterol efflux pathways should be explored. Such molecules may hold great promise given the central role of IL-1β in the development of atherosclerosis.

STAR★METHODS

Detailed methods are provided in the online version of this paper and include the following:

- KEY RESOURCES TABLE
- RESOURCE AVAILABILITY
  - Lead Contact
  - Materials Availability
  - Data and Code Availability
- EXPERIMENTAL MODEL AND SUBJECT DETAILS
  - Primary cell cultures
  - Atheroma plaque samples
  - Ethics statement

(C) Representative immunohistochemical staining of serial sections of human carotid arteries (n = 7) for CD68, LXR-α, HIF-1α, IL-1β, and negative control (without primary antibody). Magnification is indicated on each picture.
(D) Co-immunostaining of LXR-α (red) and CD68 (green). Nuclei are stained with DAPI.
(E) Co-immunostaining of HIF-1α (green) and LXR-α (red). Nuclei are stained with DAPI. Pictures are representative of different plaques samples.
See also Figures S8 and S9 and Table S1.

SUPPLEMENTAL INFORMATION

Supplemental Information can be found online at https://doi.org/10.1016/j.celrep.2020.107665.

ACKNOWLEDGMENTS

We thank Audrey Geissler and André Bouchot from the DImaCell core facility, INSERM U1231 CellmaP site, the flow cytometry facility, and Victoria Bergas and Hélène Choubley from the lipidomic analytic platform for expert technical assistance. This work was supported by grants from CHU Dijon, Region Bourgogne-Franche Comté, the European Regional Development Fund, the University of Burgundy, Institut National de la Santé et de la Recherche Médicale (INSERM), and by a French government grant managed by the French National Research Agency under the program "Investissements d'Avenir" with reference ANR-11-LABX-0021 (LipSTIC Labex).

AUTHOR CONTRIBUTIONS

Conceptualization, D.M. and L.M.; Methodology, D.M., C.T., and L.M.; Investigation, L.M., A.J., J.B.J., C.M., V.D., A.C., L.B., A.D., M.J.M., and J.-P.P.; Writing – Original Draft, D.M., C.T., and L.M.; Writing – Review & Editing, L.L., P.S., C.R., W.L., and N.V.; Funding Acquisition, L.L. and D.M.; Resources, E.S., V.C., and A.L.; Supervision, D.M.

DECLARATION OF INTERESTS

The authors declare no competing interests.

Received: May 21, 2019
Revised: January 9, 2020
Accepted: April 28, 2020
Published: May 19, 2020

REFERENCES

Bolger, A.M., Lohse, M., and Usadel, B. (2014). Trimmomatic: a flexible trimmer for Illumina sequence data. Bioinformatics *30*, 2114–2120.

Bonello, S., Zähringer, C., BelAiba, R.S., Djordjevic, T., Hess, J., Michiels, C., Kietzmann, T., and Görlach, A. (2007). Reactive oxygen species activate the HIF-1alpha promoter via a functional NFkappaB site. Arterioscler. Thromb. Vasc. Biol. *27*, 755–761.

Duewell, P., Kono, H., Rayner, K.J., Sirois, C.M., Vladimer, G., Bauernfeind, F.G., Abela, G.S., Franchi, L., Nuñez, G., Schnurr, M., et al. (2010). NLRP3 inflamasomes are required for atherogenesis and activated by cholesterol crystals that form early in disease. Nature *464*, 1357–1361.

Feldmann, R., Fischer, C., Kodelja, V., Behrens, S., Haas, S., Vingron, M., Timmermann, B., Geikowski, A., and Sauer, S. (2013). Genome-wide analysis of LXRα activation reveals new transcriptional networks in human atherosclerotic foam cells. Nucleic Acids Res. *41*, 3518–3531.

Folco, E.J., Sheikine, Y., Rocha, V.Z., Christen, T., Shvartz, E., Sukhova, G.K., Di Carli, M.F., and Libby, P. (2011). Hypoxia but not inflammation augments glucose uptake in human macrophages: Implications for imaging atherosclerosis with 18fluorine-labeled 2-deoxy-D-glucose positron emission tomography. J. Am. Coll. Cardiol. *58*, 603–614.

Folco, E.J., Sukhova, G.K., Quillard, T., and Libby, P. (2014). Moderate hypoxia potentiates interleukin-1β production in activated human macrophages. Circ. Res. *115*, 875–883.

Fontaine, C., Rigamonti, E., Nohara, A., Gervois, P., Teissier, E., Fruchart, J.-C., Staels, B., and Chinetti-Gbaguidi, G. (2007). Liver X receptor activation potentiates the lipopolysaccharide response in human macrophages. Circ. Res. *101*, 40–49.

Ghisletti, S., Huang, W., Ogawa, S., Pascual, G., Lin, M.-E., Willson, T.M., Rosenfeld, M.G., and Glass, C.K. (2007). Parallel SUMOylation-dependent pathways mediate gene- and signal-specific transrepression by LXRs and PPARgamma. Mol. Cell *25*, 57–70.

Hong, C., and Tontonoz, P. (2014). Liver X receptors in lipid metabolism: opportunities for drug discovery. Nat. Rev. Drug Discov. *13*, 433–444.

Huang, W., Sherman, B.T., and Lempicki, R.A. (2009). Systematic and integrative analysis of large gene lists using DAVID bioinformatics resources. Nat. Protoc. *4*, 44–57.

Ishibashi, M., Filomenko, R., Rébé, C., Chevriaux, A., Varin, A., Derangère, V., Bessède, G., Gambert, P., Lagrost, L., and Masson, D. (2013). Knock-down of the oxysterol receptor LXRα impairs cholesterol efflux in human primary macrophages: lack of compensation by LXRβ activation. Biochem. Pharmacol. *86*, 122–129.

Ito, A., Hong, C., Rong, X., Zhu, X., Tarling, E.J., Hedde, P.N., Gratton, E., Parks, J., and Tontonoz, P. (2015). LXRs link metabolism to inflammation through Abca1-dependent regulation of membrane composition and TLR signaling. eLife *4*, e08009.

Joseph, S.B., Castrillo, A., Laffitte, B.A., Mangelsdorf, D.J., and Tontonoz, P. (2003). Reciprocal regulation of inflammation and lipid metabolism by liver X receptors. Nat. Med. *9*, 213–219.

Kase, E.T., Wensaas, A.J., Aas, V., Højlund, K., Levin, K., Thoresen, G.H., Beck-Nielsen, H., Rustan, A.C., and Gaster, M. (2005). Skeletal muscle lipid accumulation in type 2 diabetes may involve the liver X receptor pathway. Diabetes *54*, 1108–1115.

Kirchgessner, T.G., Sleph, P., Ostrowski, J., Lupisella, J., Ryan, C.S., Liu, X., Fernando, G., Grimm, D., Shipkova, P., Zhang, R., et al. (2016). Beneficial and adverse effects of an LXR agonist on human lipid and lipoprotein metabolism and circulating neutrophils. Cell Metab. *24*, 223–233.

Koslowski, M., Luxemburger, U., Türeci, O., and Sahin, U. (2011). Tumor-associated CpG demethylation augments hypoxia-induced effects by positive autoregulation of HIF-1α. Oncogene *30*, 876–882.

Libby, P., Ridker, P.M., and Hansson, G.K.; Leducq Transatlantic Network on Atherothrombosis (2009). Inflammation in atherosclerosis: from pathophysiology to practice. J. Am. Coll. Cardiol. *54*, 2129–2138.

Monaco, C., Gregan, S.M., Navin, T.J., Foxwell, B.M.J., Davies, A.H., and Feldmann, M. (2009). Toll-like receptor-2 mediates inflammation and matrix degradation in human atherosclerosis. Circulation *120*, 2462–2469.

Moreno-Manzano, V., Rodríguez-Jiménez, F.J., Aceña-Bonilla, J.L., Fustero-Lardíes, S., Erceg, S., Dopazo, J., Montaner, D., Stojkovic, M., and Sánchez-Puelles, J.M. (2010). FM19G11, a new hypoxia-inducible factor (HIF) modulator, affects stem cell differentiation status. J. Biol. Chem. *285*, 1333–1342.

Morgan, M.J., and Liu, Z.G. (2011). Crosstalk of reactive oxygen species and NF-κB signaling. Cell Res. *21*, 103–115.

Muse, E.D., Yu, S., Edillor, C.R., Tao, J., Spann, N.J., Troutman, T.D., Seidman, J.S., Henke, A., Roland, J.T., Ozeki, K.A., et al. (2018). Cell-specific

discrimination of desmosterol and desmosterol mimetics confers selective regulation of LXR and SREBP in macrophages. Proc. Natl. Acad. Sci. U S A *115*, E4680–E4689.

Na, T.-Y., Lee, H.-J., Oh, H.-J., Huh, S., Lee, I.-K., and Lee, M.-O. (2011). Positive cross-talk between hypoxia inducible factor-1α and liver X receptor α induces formation of triglyceride-loaded foam cells. Arterioscler. Thromb. Vasc. Biol. *31*, 2949–2956.

Nishizawa, T., Kanter, J.E., Kramer, F., Barnhart, S., Shen, X., Vivekanandan-Giri, A., Wall, V.Z., Kowitz, J., Devaraj, S., O'Brien, K.D., et al. (2014). Testing the role of myeloid cell glucose flux in inflammation and atherosclerosis. Cell Rep. *7*, 356–365.

Novakovic, B., Habibi, E., Wang, S.-Y., Arts, R.J.W., Davar, R., Megchelenbrink, W., Kim, B., Kuznetsova, T., Kox, M., Zwaag, J., et al. (2016). β-Glucan reverses the epigenetic state of LPS-induced immunological tolerance. Cell *167*, 1354–1368.e14.

Oishi, Y., Hayashi, S., Isagawa, T., Oshima, M., Iwama, A., Shimba, S., Okamura, H., and Manabe, I. (2017). Bmal1 regulates inflammatory responses in macrophages by modulating enhancer RNA transcription. Sci. Rep. *7*, 7086.

Parathath, S., Mick, S.L., Feig, J.E., Joaquin, V., Grauer, L., Habiel, D.M., Gassmann, M., Gardner, L.B., and Fisher, E.A. (2011). Hypoxia is present in murine atherosclerotic plaques and has multiple adverse effects on macrophage lipid metabolism. Circ. Res. *109*, 1141–1152.

Park, S.H., Kang, K., Giannopoulou, E., Qiao, Y., Kang, K., Kim, G., Park-Min, K.-H., and Ivashkiv, L.B. (2017). Type I interferons and the cytokine TNF cooperatively reprogram the macrophage epigenome to promote inflammatory activation. Nat. Immunol. *18*, 1104–1116.

Pehkonen, P., Welter-Stahl, L., Diwo, J., Ryynänen, J., Wienecke-Baldacchino, A., Heikkinen, S., Treuter, E., Steffensen, K.R., and Carlberg, C. (2012). Genome-wide landscape of liver X receptor chromatin binding and gene regulation in human macrophages. BMC Genomics *13*, 50.

Pourcet, B., Gage, M.C., León, T.E., Waddington, K.E., Pello, O.M., Steffensen, K.R., Castrillo, A., Valledor, A.F., and Pineda-Torra, I. (2016). The nuclear receptor LXR modulates interleukin-18 levels in macrophages through multiple mechanisms. Sci. Rep. *6*, 25481.

Rébé, C., Raveneau, M., Chevriaux, A., Lakomy, D., Sberna, A.-L., Costa, A., Bessède, G., Athias, A., Steinmetz, E., Lobaccaro, J.M.A., et al. (2009). Induction of transglutaminase 2 by a liver X receptor/retinoic acid receptor alpha pathway increases the clearance of apoptotic cells by human macrophages. Circ. Res. *105*, 393–401.

Ridker, P.M., Everett, B.M., Thuren, T., MacFadyen, J.G., Chang, W.H., Ballantyne, C., Fonseca, F., Nicolau, J., Koenig, W., Anker, S.D., et al.; CANTOS Trial Group (2017). Antiinflammatory therapy with canakinumab for atherosclerotic disease. N. Engl. J. Med. *377*, 1119–1131.

Sarrazy, V., Viaud, M., Westerterp, M., Ivanov, S., Giorgetti-Peraldi, S., Guinamard, R., Gautier, E.L., Thorp, E.B., De Vivo, D.C., and Yvan-Charvet, L. (2016). Disruption of Glut1 in hematopoietic stem cells prevents myelopoiesis and enhanced glucose flux in atheromatous plaques of ApoE(-/-) mice. Circ. Res. *118*, 1062–1077.

Schneider, C.A., Rasband, W.S., and Eliceiri, K.W. (2012). NIH Image to ImageJ: 25 years of image analysis. Nat. Methods *9*, 671–675.

Sluimer, J.C., Gasc, J.-M., van Wanroij, J.L., Kisters, N., Groeneweg, M., Sollewijn Gelpke, M.D., Cleutjens, J.P., van den Akker, L.H., Corvol, P., Wouters, B.G., et al. (2008). Hypoxia, hypoxia-inducible transcription factor, and macrophages in human atherosclerotic plaques are correlated with intraplaque angiogenesis. J. Am. Coll. Cardiol. *51*, 1258–1265.

Spann, N.J., Garmire, L.X., McDonald, J.G., Myers, D.S., Milne, S.B., Shibata, N., Reichart, D., Fox, J.N., Shaked, I., Heudobler, D., et al. (2012). Regulated accumulation of desmosterol integrates macrophage lipid metabolism and inflammatory responses. Cell *151*, 138–152.

Stewart, C.R., Stuart, L.M., Wilkinson, K., van Gils, J.M., Deng, J., Halle, A., Rayner, K.J., Boyer, L., Zhong, R., Frazier, W.A., et al. (2010). CD36 ligands promote sterile inflammation through assembly of a Toll-like receptor 4 and 6 heterodimer. Nat. Immunol. *11*, 155–161.

Tall, A.R., and Yvan-Charvet, L. (2015). Cholesterol, inflammation and innate immunity. Nat. Rev. Immunol. *15*, 104–116.

Tannahill, G.M., Curtis, A.M., Adamik, J., Palsson-McDermott, E.M., McGettrick, A.F., Goel, G., Frezza, C., Bernard, N.J., Kelly, B., Foley, N.H., et al. (2013). Succinate is an inflammatory signal that induces IL-1β through HIF-1α. Nature *496*, 238–242.

Thomas, D.G., Doran, A.C., Fotakis, P., Westerterp, M., Antonson, P., Jiang, H., Jiang, X.-C., Gustafsson, J.-Å., Tabas, I., and Tall, A.R. (2018). LXR suppresses inflammatory gene expression and neutrophil migration through cis-repression and cholesterol efflux. Cell Rep. *25*, 3774–3785.e4.

Töröcsik, D., Baráth, M., Benko, S., Széles, L., Dezso, B., Póliska, S., Hegyi, Z., Homolya, L., Szatmári, I., Lányi, A., and Nagy, L. (2010). Activation of liver X receptor sensitizes human dendritic cells to inflammatory stimuli. J. Immunol. *184*, 5456–5465.

Tripathi, S., Pohl, M.O., Zhou, Y., Rodriguez-Frandsen, A., Wang, G., Stein, D.A., Moulton, H.M., DeJesus, P., Che, J., Mulder, L.C.F., et al. (2015). Meta- and orthogonal integration of influenza "omics" data defines a role for UBR4 in virus budding. Cell Host Microbe *18*, 723–735.

Ugocsai, P., Hohenstatt, A., Paragh, G., Liebisch, G., Langmann, T., Wolf, Z., Weiss, T., Groitl, P., Dobner, T., Kasprzak, P., et al. (2010). HIF-1beta determines ABCA1 expression under hypoxia in human macrophages. Int. J. Biochem. Cell Biol. *42*, 241–252.

Venteclef, N., Jakobsson, T., Ehrlund, A., Damdimopoulos, A., Mikkonen, L., Ellis, E., Nilsson, L.-M., Parini, P., Jänne, O.A., Gustafsson, J.-A., et al. (2010). GPS2-dependent corepressor/SUMO pathways govern anti-inflammatory actions of LRH-1 and LXRbeta in the hepatic acute phase response. Genes Dev. *24*, 381–395.

Walczak, R., Joseph, S.B., Laffitte, B.A., Castrillo, A., Pei, L., and Tontonoz, P. (2004). Transcription of the vascular endothelial growth factor gene in macrophages is regulated by liver X receptors. J. Biol. Chem. *279*, 9905–9911.

Wang, B., and Tontonoz, P. (2018). Liver X receptors in lipid signalling and membrane homeostasis. Nat. Rev. Endocrinol. *14*, 452–463.

Westerterp, M., Fotakis, P., Ouimet, M., Bochem, A.E., Zhang, H., Molusky, M.M., Wang, W., Abramowicz, S., la Bastide-van Gemert, S., Wang, N., et al. (2018). Cholesterol efflux pathways suppress inflammasome activation, NETosis, and atherogenesis. Circulation *138*, 898–912.

Zhang, W., Petrovic, J.-M., Callaghan, D., Jones, A., Cui, H., Howlett, C., and Stanimirovic, D. (2006). Evidence that hypoxia-inducible factor-1 (HIF-1) mediates transcriptional activation of interleukin-1beta (IL-1beta) in astrocyte cultures. J. Neuroimmunol. *174*, 63–73.

Zuercher, W.J., Buckholz, R.G., Campobasso, N., Collins, J.L., Galardi, C.M., Gampe, R.T., Hyatt, S.M., Merrihew, S.L., Moore, J.T., Oplinger, J.A., et al. (2010). Discovery of tertiary sulfonamides as potent liver X receptor antagonists. J. Med. Chem. *53*, 3412–3416.

STAR★METHODS

KEY RESOURCES TABLE

REAGENT or RESOURCE	SOURCE	IDENTIFIER
Antibodies		
goat polyclonal anti-IL1 beta	RD Systems	Cat#AF201SP; RRID:AB_354387
Mouse HRP-conjugated polyclonal anti-goat	Agilent-Dako	Cat#P044701-2; RRID:AB_2617137
Mouse monoclonal anti-LXRalpha/NR1H3 (clone OTI1A5)	Novus Biologicals	Cat#NBP2-46220
Rabbit monoclonal anti-HIF-1alpha (clone EP1215Y)	Abcam	Cat#Ab51608; RRID:AB_880418
Mouse monoclonal anti-CD68 (KP1)	Invitrogen	Cat#14-0688-82; RRID:AB_11151139
Mouse monoclonal anti-human IL-1β (clone B-A15)	Diaclone	Cat#855.010.005; RRID:AB_1587095
Mouse monoclonal anti-HIF-1alpha (clone 54-HIF-1α)	BD Biosciences	Cat#610958; RRID:AB_398271
Rabbit polyclonal anti-HIF-1alpha	Novus Biologicals	Cat#NB100-134SS; RRID:AB_350071
Alexa fluor 568 IgG1 Goat anti-mouse	Life Technologies	Cat#A211-24; RRID:AB_2535766
Alexa fluor 568 IgG1 Goat anti-rabbit	Life Technologies	Cat#A110-11; RRID:AB_143157
Alexa fluor 488 phalloidin	Life Technologies	Cat#A12379
Mouse monoclonal anti-Nf-kB p65 (pS536) (clone J144-460 RUO)	BD Biosciences	Cat#558377; RRID:AB_647285
Alexa fluor 555 IgG (H+L) Goat anti-mouse	ThermoFisher Scientific	Cat#A28180; RRID:AB_2536164
Dynabeads M-280 Sheep Anti-Rabbit IgG	ThermoFisher Scientific	Cat#11203D ; RRID:AB_2783009
Dynabeads M-280 Sheep Anti-Mouse IgG	ThermoFisher Scientific	Cat#11201D; RRID:AB_2783640
Mouse monoclonal anti-HIF-1alpha (clone H1alpha67)	Novus Biologicals	Cat#NB100-105; RRID:AB_10001154
Rabbit polyclonal anti-Histone H3ac (pan-acetyl)	Active Motif	Cat#61638; RRID:AB_2793714
Rabbit polyclonal anti-LXRalpha (pAb)	Active Motif	Cat#61175; RRID:AB_2614981
Rabbit Anti-HIF-1 alpha antibody - ChIP Grade (ab2185)	Abcam	Cat#ab2185; RRID:AB_302883
Alexa fluor 488 IgG (H+L) Goat anti-rabbit	ThermoFisher Scientific	Cat#A-11034; RRID:AB_2576217
CF Dye 568 IgG (H+L) Goat anti-mouse	Biotium	Cat#20100 ; RRID:AB_10559038
Alexa fluor 488 IgG (H+L) Rabbit anti-mouse	ThermoFisher Scientific	Cat#A-11059; RRID:AB_2534106
Biological Samples		
Human carotid atheroma plaques	University Hospital of Dijon: department of Cardiovascular Surgery	MASCADI Study NCT03202823
Chemicals, Peptides, and Recombinant Proteins		
Macrophage-Colony Stimulating Factor	Miltenyi Biotec	Cat#130-093-963
GW3965	Sigma-Aldrich	Cat#405911-17-3
FM19G11	Sigma-Aldrich	Cat#329932-55-0
diméthylsulfoxide	Sigma-Aldrich	Cat#D8418
Adenosine 5′-triphosphate disodium salt hydrate	Sigma-Aldrich	Cat#34369-07-8
Lipopolysaccharide (E.*coli* 055:B5)	Sigma-Aldrich	Cat#E8029-1VL
GSK2033	Sigma-Aldrich	Cat#1221277-90-2
T0901317	Cayman chemical	Cat#293754-55-9
Pam3CSK4	InvivoGen	Cat#tlrl-pms

(*Continued on next page*)

Continued

REAGENT or RESOURCE	SOURCE	IDENTIFIER
RNaseOUT Recombinant Ribonuclease Inhibitor	Invitrogen	Cat#10777019
HEPES Buffer 1M	ThermoFisher Scientific	Cat#A-15630049
Sodium pyruvate (100mM)	ThermoFisher Scientific	Cat#A-11360070
IGEPAL® CA-630	Sigma-Aldrich	Cat#I8896
4'6-diamino-2-phenylindole	ThermoFisher Scientific	Cat#D1306
Trimethylsilyl 2,2,2-trifluoro-N-(trimethylsilyl)acetimidate	ThermoFisher Scientific	Cat#11776957
Cyanine 3-CTP	Perkin Elmer	NEL580001EA
RNase A	ThermoFisher Scientific	Cat#R1253
Proteinase K Solution	ThermoFisher Scientific	Cat#4333793
25-OH-cholesterol-d6	Avanti Polar Lipids	Cat#700053
27-OH-cholesterol-d6	Avanti Polar Lipids	Cat#700059
7-α-OH-cholesterol-d7	Avanti Polar Lipids	Cat#700043
7-β-OH-cholesterol-d7	Avanti Polar Lipids	Cat#700044
7-keto-OH-cholesterol-d7	Avanti Polar Lipids	Cat#700046
lanosterol-d6	Avanti Polar Lipids	Cat#700090
epicoprostanol	Sigma-Aldrich	Cat#516-92-17
22(R)-hydroxy-cholesterol	Cayman Chemical	Cat#17954-98-2
Critical Commercial Assays		
Monocyte Isolation Kit II	Miltenyi Biotec	Cat#130-117-337
Lipofectamine® RNAiMAX Transfection Reagent	Invitrogen	Cat#13778150
RNeasy Mini Kit	QIAGEN	Cat#74106
M-MLV Reverse Transcriptase (200 U/μL)	Invitrogen	Cat#28025013
Fast SYBR Green Master Mix	Invitrogen	Cat#4385612
Pierce ECL Western Blotting Substrate	ThermoFisher Scientific	Cat#32209
Seahorse XF Glycolytic Rate Assay Kit	Agilent Technologies	Cat#103344-100
Human/Mouse Total HIF-1 alpha DuoSet IC ELISA	RD Systems	Cat#DYC1935-2
BD Cytometric Bead Array (CBA) Human Inflammatory Cytokines Kit	BD Biosciences	Cat#551811
Human IL-1beta ELISA Kit	Sigma-Aldrich	Cat#RAB0273
Gene Expression Microarray Hybridization Kit	Agilent Technologies	Cat#51885242
ChIP DNA Clean & Concentrator(Capped Columns)	Zymo Research	Cat#D5205
Low Input Quick Amp Gene Expression Labeling Kits	Agilent Technologies	Cat#51902305
Deposited Data		
Raw and analyzed data	Rébé et al., 2009	GEO: GSE13407
Raw and analyzed data	This paper	GEO: GSE125126
Experimental Models: Cell Lines		
Human: peripheral blood monocytes	Etablissement Français du Sang: healthy donors	N/A
Mouse: bone-marrow derived monocytes	*Mus musculus* C57Bl6J	Protocol no. 2017010214489525_v2#8381
Oligonucleotides		
siRNA targeting sequence: *NR1H3* (s19568)	Ambion, Invitrogen	Cat#4390824
siRNA targeting sequence: *HIF1alpha* (s6541)	Ambion, Invitrogen	Cat#4390824

(*Continued on next page*)

Continued

REAGENT or RESOURCE	SOURCE	IDENTIFIER
All primers are available in Table S2	Eurogentec	N/A
Software and Algorithms		
Seahorse XFe96 Software Wave Desktop	Agilent Technologies	https://www.agilent.com/en/products/cell-analysis/software-download-for-wave-desktop
ImageJ	Schneider et al., 2012	https://imagej.nih.gov/ij/
Trimmomatic	Bolger et al., 2014	http://www.usadellab.org/cms/?page=trimmomatic
Other		
Metascape	Tripathi et al., 2015	www.metascape.org
DAVID	Huang et al., 2009	https://david.ncifcrf.gov/

RESOURCE AVAILABILITY

Lead Contact

Further information and requests for resources and reagents should be directed to and will be fulfilled by the Lead Contact, David Masson (david.masson@chu-dijon.fr).

Materials Availability

This study did not generate new unique reagents.

Data and Code Availability

Microarray and RNA seq data discussed in this publication have been deposited in NCBI's Gene Expression Omnibus The accession number for the data reported in this paper are GEO:GSE13407 and GEO:GSE125126.

EXPERIMENTAL MODEL AND SUBJECT DETAILS

Primary cell cultures

Human Peripheral-blood Monocytes were obtained from healthy, buffy coats from male and female healthy anonymous donors by the Etablissement Français du Sang (Besançon, France). Mononuclear cells were isolated by Ficoll gradient centrifugation and monocyte negative selection was performed via magnetic activated cell sorting using the Monocyte Isolation Kit II (Miltenyi Biotec) according to the manufacturer's instructions as previously described (Rébé et al., 2009). Bone marrow cells were isolated from tibias and femurs from WT mice on pure C57Bl6J background (male and female mice from 15 to 30 weeks old were used). Cells were collected from bone marrow, centrifugated (300 g, 10min,4°C) and washed with PBS. Cells were resuspended in PBS w/o Ca^{2+}-Mg2+ containing FcR blocking reagent according to manufacturer's instructions (Miltenyi Biotec). Cells were then immunostained with CD115-PE antibody according to manufacturer's instructions (Miltenyi Biotec). CD115 positive cells corresponding to bone marrow derived monocytes were sorted using a BD FACS ARIA III flow cytometer (Becton Dickinson).

Human or murine monocytes were differentiated into macrophages for 6 days with 100 ng/mL of M-CSF into RPMI medium (GIBCO, Fisher Scientific) supplemented with 10% Fetal Bovine Serum (FBS) in 5% CO2 and 37°C. On day 6, macrophages were treated with or without 1 μM of synthetic LXR agonist GW3965 (Sigma Aldrich) for 48 hours and then with or without 100 ng/mL of TLR2 agonist Pam3CSK4 (InvivoGen) or 100 ng/mL of LPS (*E.coli* 055:B5) for 4 hours.

Atheroma plaque samples

Atheroma plaque samples were obtained from patients undergoing carotid endarterectomy at the Department of Cardiovascular Surgery at the University Hospital of Dijon. Lipid rich cores of plaque samples were carefully dissected under aseptic conditions and were homogenized with 3 volumes of cold NaCl 150 mmol/L and briefly sonicated. Macrophages were treated with whole homogenate (1% v/v in cell culture medium) for 48 hours with or without 1 μM GSK2033 (Sigma Aldrich). Based on the cholesterol content of plaque homogenates (approx. 50 nmol/mg), we used a 1/100 dilution that led to an approx. final concentration of 0.5 μmol/ml cholesterol in the culture medium. Similar cholesterol concentrations are typically used for cholesterol loading of macrophages with acetylated LDL (100-200 μg/ml cholesterol).

Ethics statement

Human peripheral blood was collected from healthy donors following informed consent, provide in accordance with the Declaration of Helsinki by the Etablissement Français du Sang (Besançon, France).

All of the animal experimental procedures were conducted in accordance with the local guidelines for animal experimentation. Protocol no. 2017010214489525_v2#8381 was approved by the Animal Care and Use Committee of the University of Burgundy.

Atheroma plaque samples were obtained from patients undergoing carotid endarterectomy at the Department of Cardiovascular Surgery at the University Hospital of Dijon (Burgundy, France) (MASCADI STUDY NCT03202823). All patients provided an informed consent and the study was approved by the local ethic committee (CPP 17.02.05).

METHOD DETAILS

Gene silencing

For transfection experiment, on day 6, macrophages were transfected with negative siRNAs (Ambion, Invitrogen) or siRNA for *NR1H3* (Ambion, Invitrogen) (ID: s19568) or siRNA for *HIF1A* (Ambion, Invitrogen) (ID: s6541) using Lipofectamine® RNAiMAX (Invitrogen) according to the manufacturer's instructions. During transfection cells were treated with or without 1 μM of synthetic LXR agonist GW3965 for 48 hours and then with or without 100 ng/mL of TLR2 agonist Pam3CSK4 or 100 ng/mL LPS.

Gene expression analysis

Total RNA was extracted using RNeasy Mini Kit (QIAGEN) according to the manufacturer's instructions. 100 ng of total RNA was reverse transcribed using M-MLV Reverse Transcriptase, random primers and RNaseOUT inhibitor (Invitrogen). cDNA obtained were quantified by real time PCR using SYBR Green RT-PCR Kit (Invitrogen)) and using a StepOne Plus Real-Time PCR System (Applied Biosystems). ΔΔCt method was used to determine the relative mRNA levels of each gene and Ct were normalized using Cyclophilin A or 36B4 mRNA levels for human and *Gapdh* mRNA levels for mouse. In bar graphs, data are normalized at 1 in the control group. In dot plots, the expression is normalized to the mean of the basal gene expression from the different donors.

Protein lysate and immunoblotting

Total cellular protein extract were prepared with RIPA buffer and protease inhibitor cocktails. Protein lysates were separated by Sodium Dodecyl Sulfate gel electrophoresis (SDS-PAGE) and transferred to nitrocellulose membrane (Schleicher and Schuell). After incubation for 2 hours at RT with 5% nonfat milk in Tris-Buffered Saline (TBS)-0.1% Tween 20, membranes were incubated overnight with the primary antibody Human IL-1 beta (AF201SP, IgG goat polyclonal, RD Systems) 1/500 diluted in 1% BSA-TBS-Tween, washed, incubated with the secondary antibody HRP-conjugated polyclonal mouse anti-goat immunoglobulins (Dako P044701-2) for 30 min. at RT, and washed again before analysis with luminol reagent Pierce ECL Western Blotting Substrate (Thermo Fisher Scientific).

Metabolic flux analysis

Proton exchange rate (PER) in macrophages were measured at 37°C using the Seahorse XFe96 Extracellular Flux Analyzer instrument (Seahorse Bioscience, Agilent) and the XF Glycolytic Rate Assay Kit (Agilent Part number 103344-100). Briefly, after treatment with or without 1μM synthetic LXR agonist GW3965 for 48 hours, cells were seeded in a 24-well culture plate XFe96 FluxPak (Agilent) at a density of 30,000 cells per well for 24 hours in the same medium and treated or not with 100 ng/mL TLR2 agonist Pam3CSK4 for 4 hours. Cells were then changed to XF DMEM Base Medium without Phenol Red (Agilent Part number 103335-100) supplement with 5 mM HEPES, 10 mM glucose,1 mM sodium pyruvate, 2 mM glutamine, pH 7.4 at 37°C. After cells incubated for 1 hour at 37°C in a non-CO2 incubator, respiration and acidification of the medium was measured before and after the injection of two compounds: 0.5 μM rotenone + 0.5 μM antimycin A (first injection) and 50 mM 2-deoxy-D-glucose (second injection). Experiments were performed in real time in eight replicate wells for each cell line. PER, OCR and ECAR were automatically calculated by the Seahorse XFe96 software (Seahorse Bioscience, Agilent).

Biochemical analysis

Total HIF-1α concentrations were determined by a commercially available ELISA Kit (Human/Mouse Total HIF-1α, DYC1935-2, RD Systems) in accordance with the manufacturer's protocols. Cytokine medium levels were measured by BD Cytometric Bead Array (CBA) Human Inflammatory Cytokines Kit according to the manufacturer's protocols, and using a Flow Cytometer FACSCanto-123 apparatus (BD Biosciences), and by commercially available ELISA Kit for IL-1β (Human IL-1 beta ELISA Kit, RAB0273-1KT, Sigma Aldrich).

Carotid plaques immunohistological analysis

The plaque samples were fixed in neutral buffered formalin, dehydrated in graded alcohols, cleared in xylene and embedded in paraffin. Slices of 5 μm thick were deposited on slide to achieve a hematoxylin–eosin staining and immunohistochemical analysis. Automated immunohistochemistry (Leica BondMax) was performed using standard procedures on serial sections of plaques. The following antibodies were used: anti-LXRα/NR1H3 antibody (OTI1A5) (NBP2-46220, mouse monoclonal, 1/200) (Novus Biologicals), anti-HIF-1 alpha (EP1215Y) (ab51608, rabbit monoclonal, 1/100) (Abcam), anti-CD68 antibody (14-0688-82, mouse monoclonal, 1/200) (Invitrogen), anti-human IL-1β azide free (Clone B-A15) (855.010.005, mouse monoclonal IgG1, 1/50) (Diaclone). For co-localization experiments, same primary antibodies were used used: LXRα/NR1H3 antibody (OTI1A5) (1:50), anti-HIF-1 alpha antibody

(EP1215Y) (1:50) and anti-CD68 antibody (1:100) (Invitrogen). Revelation was made using the following secondary antibodies: goat anti-rabbit IgG Alexa Fluor 488 (Invitrogen, #A11034, 1:500) or goat anti-mouse CF Dye 568 (Biotium, #20100., 1:500) or rabbit anti-mouse Alexa Fluor 488 (Invitrogen, #A11059, 1:500).

Immunofluorescence imaging

Characterization and localization of HIF-1α

The macrophages growing in Labtech culture chamber were washed in PBS and fixed in 4% paraformaldehyde (PFA) (4°C, 30min). After fixation cells were permeabilized 10 min using 0.2% Triton X-100 in PBS, washed in PBS and then blocked for 1 hour in 20% of PBS-Foetal Bovin Serum (FBS) (GIBCO, Fisher Scientific). Immunolabellings were then processed. For human HIF-1α staining, a mouse monoclonal anti- HIF-1α antibody (clone 54-HIF-1α, BD Biosciences) (1:500 in 20% of PBS-FBS) was added, for murine HIF-1α staining a rabbit polyclonal anti-HIF-1α antibody (NB100-134SS, Novus Biologicals) was added, and cells were incubated 1 hour at room temperature. After washing three time with 20% of PBS-FBS, macrophages were incubated for 45 min in the dark with an Alexa-Fluor 568 goat anti-mouse IgG1 antibody (Life Technologies A211-24) (1:500 in 20% of PBS-FBS) or goat anti-rabbit IgG1 antibody (Life Technologies A110-11) (1:500 in 20% of PBS-FBS). Finally, they were washed three times with 20% of PBS-FBS. Cells were then incubated in the dark overnight at 4°C with a combination of Alexa-Fluor 488 Phalloidin (Life Technologies A123-79) (1:500 in 20% of PBS-FBS) to stain F-actin and 4'6-diamidino-2-phenylindole (DAPI) (Life Technologies) (1 μg/mL in 20% of PBS-FBS) to stain nuclei. Cells were finally washed three times in PBS and one time in dH2O and mounted using ProLong® Gold antifade reagent (Life Technologies). Slides were examined with a BX51 epifluorescence microscope (Olympus) coupled with the 'CellF' software and using the objective 'UPlanFL 60 × /1.25 oil'. All captured images were exported to ImageJ for figure assembly (Schneider et al., 2012).

Characterization and localization of pRelA

Phosphorylated NF-κB p65 (pRelA) analysis was performed after 48 hours LXR agonist treatment of macrophages. Cells were cultured onto glass microscope slides and then were fixed and permeabilized in a methanol bath (20 min at −20°C), washed 3 times and incubated, overnight at +4°C, with the primary antibody ((Phosphor-S536 p65 (RelA) NF-κB subunit 558377) (BD Biosciences). Slides were washed 3 times with 0.5% FCS/PBS solution, and incubated 1 hour with Alexa fluor 555-conjugated Goat anti-mouse IgG antibody (H+L) (Thermo-Fisher Scientific,#A28180). Slides were washed and mounted with Mounting Media with DAPI (Sigma Aldrich). Fluorescent images were acquired on an FV1000 confocal microscope (Olympus) and analyzed with Olympus FVviewer software.

Microarray Procedures

RNA Amplification and Labeling

Human total RNA was isolated with the use of Trizol (Sigma-Aldrich). Sample labeling was performed as detailed in the "One-Color Microarray-Based Gene Expression Analysis" protocol (version 5.5, part number G4140-90040). Briefly, 1 μg of each total RNA samples was used for the amplification and labeling step using the Agilent Low RNA Input Linear Amp Kit (Agilent Technologies) in the presence of cyanine 3-CTP (Perkin Elmer). Yields of cRNA and the dye incorporation rate were measured with the ND-1000 Spectrophotometer (NanoDrop Technologies).

Human Genome Oligo Microarrays Hybridization

The hybridization procedure was performed according to the "One-Color Microarray-Based Gene Expression Analysis" protocol (version 5.5, part number G4140-90040) using the Agilent Gene Expression Hybridization Kit (Agilent Technologies, Santa Clara, USA). Briefly, 1.65 μg Cy3-labeled fragmented cRNA in hybridization buffer was hybridized overnight (17 hours, 65°C) to Agilent Whole Human Genome Oligo Microarrays 4x44K using Agilent's recommended hybridization chamber and oven. Following hybridization, the microarrays were washed once with 6x SSPE buffer containing 0.005% N-lauroylsarcosine for 1 min at room temperature followed by a second wash with preheated 0.06x SSPE buffer (37°C) containing 0.005% N-lauroylsarcosine for 1 min. The last washing step was performed with acetonitrile for 30 s.

Scanning and data analysis

Fluorescence signals of the hybridized Agilent Microarrays were detected using Agilent's Microarray Scanner System (Agilent Technologies). The Agilent Feature Extraction Software (FES) was used to read out and process the microarray image files.

Histone 3 acetylation measurement by Chip

Human primary macrophages were crosslinked with 1% formaldehyde in PBS for 10 min. The reaction was stopped with glycine at a final concentration of 0.125 M for 5 min. Approximately 10–20 × 10^6 cells were used for H3ac. Cells were spun down and rinsed with cold PBS two times. Nuclei were isolated using lysis buffer 1 (PIPES 500mL, KCl 80mM and IGEPAL 1%) and lysis buffer 2 (SDS 0.1%, EDTA 10mM, pH 8.1, and TrisHCL 50mM, pH 8.1), and subsequently sonicated over 45 min (30 s ON/OFF) in the Bioruptor Plus (Diagenode), to generate DNA-fragment sizes of 0.2–0.5 kb. Dynabeads® M-280 Sheep anti-Rabbit IgG or Sheep anti-Mouse IgG (ThermoFisher Scientific 11203D and 11201D) were incubated overnight with the antibodies. Each lysate was immunoprecipitated with anti-H3ac (61638, 10 μg) (Active Motif). After several washings, the beads were incubated with the sonicated chromatin overnight. On the next day, the samples were washed with RIPA buffer (50 mM HEPES-KOH pH 7.5, 200 mM NaCl, 500 mM LiCl, 1 mM EDTA, 1% NP-40, 0.7% Na-deoxycholate) six times, once with TBS (20 mM Tris-HCl pH 7.6, 150 mM NaCl), and the

immune-bound chromatin was eluted in the elution buffer (SDS 0.1%, NaHCO3 100 mM, Tris-HCl 20 mM, EDTA 5mM, NaCl 50 mM). The samples remained at 65°C overnight to reverse the formaldehyde crosslinking. After RNase A (ThermoFisher) and proteinase K (ThermoFisher) treatments, the immunoprecipitated DNA was purified using the ChIP DNA Clean & Concentrator Capped Zymo-Spin I (Zymo Research) purification kit. RT-qPCR was performed using the QuantStudio 3 Real-Time PCR Systems (ThermoFisher Scientific). qPCR on ChIP input were used for normalization of each sample result.

Chromatin immunoprecipitation

Primary macrophages cells were fixed with 1% formaldehyde for 15 min and quenched with 0.125 M glycine. Subsequent steps were performed by Active Motif. Chromatin was isolated by the addition of lysis buffer, followed by disruption with a Dounce homogenizer. Lysates were sonicated using the EpiShear Probe Sonicator (Active Motif, cat # 53051) with an EpiShear Cooled Sonication Platform (Active Motif, cat # 53080) and the DNA sheared to an average length of 300-500 bp. Genomic DNA (Input) was prepared by treating aliquots of chromatin with RNase, proteinase K and heat for de-crosslinking followed by ethanol precipitation. Pellets were resuspended and the resulting DNA was quantified on a ClarioStar spectrophotometer. Extrapolation to the original chromatin volume allowed quantitation of the total chromatin yield. Aliquots of chromatin (5 ug) were precleared with protein A agarose beads (Invitrogen). Genomic DNA regions of interest were isolated using 3 μl of antibody against LXRα (Active Motif, 61175) and HIF1α (Abcam, ab2185). Complexes were washed, eluted from the beads with SDS buffer, and subjected to RNase and proteinase K treatment. Crosslinks were reversed by incubation overnight at 65°C, and ChIP DNA was purified by phenol-chloroform extraction and ethanol precipitation. Quantitative PCR (qPCR) reactions were carried out in triplicate using SYBR Green Supermix (Bio-Rad, Cat # 170-8882) on a CFX Connect Real Time PCR system. One positive control primer pair was tested for each factor, one negative control site (Untr12 Human negative control primer pair Set 1 Catalog number 71001), plus the test sites. The resulting signals were normalized for primer efficiency by carrying out qPCR for each primer pair using input DNA (pooled unprecipitated genomic DNA from each cell line).

RNA purification for sequencing analysis

Macrophages from 3 donors each exposed to 3 distinct plaque homogenates with or without GSK2033 were used for RNA sequencing. Total RNA were prepared by using QIAGEN RNA easy kits (QIAGEN). mRNA purification from total RNA and library preparation were performed with the NEBNext Ultra RNA Library Preparation Kit with poly-A selection according to the manufacturer's protocols. Libraries were sequenced with 2x150bp paired-end reads on an Illumina HiSeq. Sequence reads were trimmed to remove possible adaptor sequences and nucleotides with poor quality using Trimmomatic v.0.36 (Bolger et al., 2014). The trimmed reads were mapped to the *Homo sapiens* GRCh38 reference genome using the STAR aligner v.2.5.2b. Unique gene hit counts were calculated by using featureCounts from the Subread package v.1.5.2. Only unique reads that fell within exon regions were counted. After extraction, the gene hit counts table was used for downstream differential expression analysis.

Sterol quantitation by GCMS

Lipid standards (25-OH-cholesterol-d6; 27-OH-cholesterol-d6; 7-α-OH-cholesterol-d7; 7-β-OH-cholesterol-d7; 7-keto-OH-cholesterol-d7; lanosterol-d6; epicoprostanol) were obtained from Avanti Polar Lipids (Coger SAS). LC-MS/MS quality grade solvents were purchased from Fischer Scientific. Other chemicals of the highest grade available were purchased from Sigma Aldrich.

Homogenates from plaques were crushed with NaCl 0.9% to obtain a plaque concentration of 0.33 mg/μL. A volume of sample corresponding to 15mg of tissue was saponified for 45min. at 56°C with 60 μL of potassium hydroxide 10 mol/L and 1.2 mL of ethanol-BHT (50 mg/L) containing 20 μL of standard-intern mix (μg/sample: 0.2 (25-OH-cholesterol-d6); 0.4 (27-OH-cholesterol-d6); 0.5 (7-α- OH-cholesterol-d7); 0.5 (7-β-OH-cholesterol-d7); 1 (7-keto-OH-cholesterol-d7); 1 (lanosterol-d6); 100 (epicoprostanol)). Sterols were extracted with 5 mL of hexane and 1mL of water. After evaporation of the organic phase, sterols were derivatized with 100 μL of a mixture of bis(trimethylsilyl)trifluoroacetamide/ trimethylchlorosilane 4/1 v/v for one hour at 80°C. After evaporation of the silylating reagent 100 μL of hexane were added. Trimethylsilylethers of sterols analysis was performed by GCMS in a 7890A gas chromatograph coupled with a 5975C Mass Detector (Agilent Technologies). Separation was achieved on a HP-5MS 30 m x 250μm column (Agilent Technologies) using helium as carrier gas and the following GC conditions: injection at 250°C using the pulsed split, oven temperature program: initial temperature 150°C up to 280°C at a rate of 15°C/min, up to 290°C at a rate of 1°C/min for 2 min. The MSD was set up as follow: EI at 70 eV mode, source temperature at 230°C. Data were acquired in SIM mode using following quantitation ions (m/z): 131.1 for 25-OH-cholesterol; 137.1 for 25-OH-cholesterol d6; 145.1 for 24(S)-OH-cholesterol; 151.1 for 24(S)-OH-cholesterol-d6; 343.3 for desmosterol; 368.3 for cholesterol; 370.3 for epicoprostanol; 375.3 for cholesterol-d7; 399.4 for lanosterol d6; 417.4 for 27-OH-cholesterol; 423.4 for 27-OH cholestrol-d6; 456.4 for 7α - 7β cholesterol; 463.5 for 7α - 7β Cholesterol-d7; 472.4 for 7-keto-cholesterol; 479.4 for 7-keto-cholesterol d7. A calibration curve was obtained with cholesterol standard (Sigma Aldrich) and desmosterol standard (Sigma Aldrich) using the same method used for samples.

QUANTIFICATION AND STATISTICAL ANALYSIS

Statistical analysis

Each experiment was performed with technical triplicate samples for one individual donor or animal. Experiments were replicated with at least two independent donors. The mean of the technical triplicates was used when combining data from independent donors.

Statistical analyses were performed using Prism 7 software (Graph-Pad) with error bars indicating the standard deviation. For datasets with 3 or more variables, a one-way or two-way ANOVA was performed followed by Sidak's multiple comparison test. For data with two variables, unpaired or paired t tests were performed. Statistical significance was defined as $p < 0.05$.

For microarray data determination of differential gene expression FES derived output data files were further analyzed using the Rosetta Resolver gene expression data analysis system (Rosetta Biosoftware).

For RNA seq analysis, a comparison of gene expression between the groups of samples was performed using DESeq2. The Wald test was used to generate p values and log2 fold changes. Genes with an adjusted p value < 0.05 and absolute log2 fold change > 1 were called as differentially expressed genes for each comparison. Correction for multiple comparison was performed using the Benjamini-Hochberg Procedure with an FDR at 5%.

Gene Ontology enrichment analysis

Significantly enriched gene ontology terms were calculated by using differentially expressed genes by using Metascape (www.metascape.org) and DAVID (Tripathi et al., 2015; Huang et al., 2009).